Association between water and carbon dioxide transport in leaf plasma membranes: assessing the role of aquaporins.

Running Title: Water and carbon dioxide transport via aquaporins

Manchun Zhao[1], Hwei-Ting Tan[1], Johannes Scharwies[1], Kara Levin[1], John R Evans[2] and Stephen D Tyerman[1]

[1] Australian Research Council Centre of Excellence in Plant Energy Biology, School of Agriculture, Food and Wine, Waite Research Institute, University of Adelaide, Glen Osmond, SA 5064, Australia

[2] Division of Plant Sciences, Research School of Biology, The Australian National University, Canberra, Australian Capital Territory 0200, Australia

Corresponding Author

Stephen D. Tyerman

Australian Research Council Centre of Excellence in Plant Energy Biology, School of Agriculture, Food and Wine, Waite Research Institute, University of Adelaide, Glen Osmond, SA 5064, Australia.

Phone: +61 8 83136663

Email: steve.tyerman@adelaide.edu.au

Abstract

The role of some aquaporins as CO_2 permeable channels has been controversial. Low CO_2 permeability of plant membranes have been criticized due to unstirred layers and other limitations. Here we measured both water and CO_2 permeability (P_{os}, P_{CO2}) using stopped flow on plasma membrane vesicles (pmv) isolated from *Pisum sativum* (pea) and *Arabidopsis thaliana* leaves. We excluded the chemical limitation of carbonic anhydrase (CA) in the vesicle acidification technique for P_{CO2} using different temperatures and CA concentrations. Unstirred layers were excluded based on small vesicle size and the positive correlation between vesicle diameter and P_{CO2}. We observed high aquaporin activity (P_{os} 0.06 to 0.22 cm s^{-1}) for pea pmv based on all the criteria for their function using inhibitors and temperature dependence. Inhibitors of P_{os} did not alter P_{CO2}. P_{CO2} ranged from 0.001 to 0.012 cm s^{-1} (mean 0.0079 $\pm$ 0.0007 cm s^{-1}) with activation energy of 30.2 kJ mol^{-1}. Intrinsic variation between pmv batches from normally grown or stressed plants revealed a weak (R^2 = 0.27) positive linear correlation between P_{os} and P_{CO2}. Despite the low P_{CO2}, aquaporins may facilitate CO_2 transport across plasma membranes, but probably via a different pathway than for water.

Introduction

Leaf mesophyll resistance to CO_2 diffusion is a significant component of the total resistance for CO_2 fixation (Evans, 1999, Flexas, Barbour, Brendel, Cabrera, Carriqui, Diaz-Espejo, Douthe, Dreyer, Ferrio, Gago, Galle, Galmes, Kodama, Medrano, Niinemets, Peguero-Pina, Pou, Ribas-Carbo, Tomas, Tosens & Warren, 2012, Warren, 2008) and can be represented as the sum of gaseous phase resistance and liquid phase resistance through the leaf (Evans, Kaldenhoff, Genty & Terashima, 2009). It is generally assumed that resistance through the gaseous phase is relatively small compared to that through the liquid phase (Niinemets & Reichstein, 2003). Among the elements that contribute to the liquid phase resistance, the apparent membrane resistance may account for more than 40% (Evans *et al.*, 2009). Carbon dioxide is lipophilic and should freely penetrate the lipid matrix of membranes resulting in extremely high permeability (Boron, Endeward, Gros, Musa-Aziz & Pohl, 2011, Missner & Pohl, 2009). As such it has been suggested that the rate limitation to diffusion is more likely to be unstirred layers adjacent to the membrane (Boron *et al.*, 2011, Gutknecht, Bisson & Tosteson, 1977, Missner & Pohl, 2009). However, biological membranes appear to have low gas permeability (either NH_3 or CO_2), for example, epithelial apical membranes (Endeward & Gros, 2005, Negrete, Lavelle, Berg, Lewis & Zeidel, 1996, Waisbren, Geibel, Modlin & Boron, 1994), and plant membranes so far measured have relatively low NH_3 (Niemietz & Tyerman, 2000) and CO_2 permeability (2-8 x 10^{-3} cm s^{-1}) (Uehlein, Otto, Hanson, Fischer, McDowell & Kaldenhoff, 2008b). This is likely to be due to sterol content (cholesterol in animals) (Endeward, Al-Samir, Itel & Gros, 2014) and/or high protein content (Boron *et al.*, 2011). If the intrinsic CO_2 permeability of the native membrane is low then proteinaceous gas channels could significantly enhance CO_2 transport.

The physiological significance of aquaporins as potential CO_2 transport facilitators in plants has been well recognised (Boron, 2010, Heckwolf, Pater, Hanson & Kaldenhoff, 2011b, Terashima & Ono, 2002b, Uehlein, Lovisolo, Siefritz & Kaldenhoff, 2003b, Uehlein, Otto, Hanson, Fischer, McDowell & Kaldenhoff, 2008a) and evidence has been accumulating that certain aquaporins can facilitate CO_2 transport (Kaldenhoff, 2012, Maurel, Boursiac, Luu, Santoni, Shahzad & Verdoucq, 2015). Cooper and Boron (1998) first demonstrated enhanced membrane permeability to CO_2 by expressing human red blood cell *AQP1* gene in *Xenopus* oocytes. That aquaporins may enhance CO_2 permeability in *Vicia faba* leaves was indicated using mercury, albeit a non-specific aquaporin inhibitor (Terashima & Ono, 2002a). The tobacco NtAQP1 (NtPIP1;2) was shown to facilitate CO_2 transport in *Xenopus* oocytes and to

alter gas exchange properties when expression was altered in leaves (Uehlein, Lovisolo, Siefritz & Kaldenhoff, 2003a). Cellular CO_2 transport in Arabidopsis appears to depend on the expression of AtPIP1;2 (Uehlein, Sperling, Heckwolf & Kaldenhoff, 2012b). Expressing aquaporins from a variety of plants in *Saccharomyces cerevisiae* has demonstrated CO_2 or NH_3 facilitated transport (Bertl & Kaldenhoff, 2007, Heinen, Bienert, Cohen, Chevalier, Uehlein, Hachez, Kaldenhoff, Le Thiec & Chaumont, 2014, Jahn, Moller, Zeuthen, Holm, Klaerke, Mohsin, Kuhlbrandt & Schjoerring, 2004, Loque, Ludewig, Yuan & von Wiren, 2005). Recently the Arabidopsis PIP2;1 aquaporin has been linked to CO_2 sensing in the guard cell through its CO_2 permeability and association with a carbonic anhydrase (Wang, Hu, Qin, Zeise, Xu, Rappel, Boron & Schroeder, 2016). The extent to which these CO_2 permeable aquaporins are also significantly water permeable appears to depend on the particular isoform, the expression system and if they form homo or heterotetramers (Otto, Uehlein, Sdorra, Fischer, Ayaz, Belastegui-Macadam, Heckwolf, Lachnit, Pede, Priem, Reinhard, Siegfart, Urban & Kaldenhoff, 2010). One of the most highly expressed CO_2 permeable aquaporins, AtPIP2;1, enhances water permeability both *in planta* and in heterologous expression systems (Grondin, Rodrigues, Verdoucq, Merlot, Leonhardt & Maurel, 2015, Wang *et al.*, 2016). Also NtAQP1 enhances both water permeability and CO_2 permeability, while AtPIP1;2 will increase CO_2 permeability but not water permeability when expressed in yeast (Heckwolf, Pater, Hanson & Kaldenhoff, 2011a). While AtPIP1;2 is clearly linked to water and CO_2 transport *in planta* (Postaire, Tournaire-Roux, Grondin, Boursiac, Morillon, Schaffner & Maurel, 2010, Uehlein *et al.*, 2012b) when ectopically expressed in lilly pollen it does not increase water permeability in contrast to AtPIP2;1 (Sommer, Geist, Da Ines, Gehwolf, Schaffner & Obermeyer, 2008). In summary, the extent to which water and CO_2 may permeate via a common or distinct set of aquaporins in the plasma membrane of photosynthetic cells will likely depend on the expression levels of particular isoforms and their associating partner aquaporins in heterotetramers or other associating proteins such as carbonic anhydrase.

Leaf mesophyll conductance to CO_2 diffusion (g_m) has been widely studied in the context of its significant limitation to the rate of CO_2 fixation (Evans *et al.*, 2009, Flexas *et al.*, 2012) but there is also a positive correlation between g_m and leaf hydraulic conductance across species to the extent that leaf hydraulic conductance can be used to predict g_m with reasonable accuracy (Flexas, Scoffoni, Gago & Sack, 2013). It has been speculated that aquaporins in leaf mesophyll cell plasma membranes may explain this correlation if the

overall activity of these aquaporins affected both leaf hydraulic conductivity (extra-xylem component) and g_m (Flexas, Scoffoni, Gago & Sack, 2013). This potential link has not been tested at the membrane level. Here we examine if there is a correlation between CO_2 permeability (P_{CO2}) and water permeability (P_{os}) of plasma membrane vesicles isolated from leaves taking into account some of the constraints that may lead to artifacts in the measurement of P_{CO2}. The temperature dependence of g_m is also important for understanding impacts of temperature on photosynthesis given the impact of g_m on photosynthesis (Flexas & Diaz-Espejo, 2015). Interestingly there is a wide variation in the temperature dependence of g_m between species (von Caemmerer & Evans, 2015). These authors modeled the temperature response based on diffusion through liquid and membrane in series to extract an activation energy for CO_2 diffusion across the leaf membranes for each species. These ranged between 36 and 76 kJ mol^{-1}, however, in the context of involvement of aquaporins in facilitating water flow, a much lower activation energy (less than about 10 kJ mol^{-1}) is used as a criterion for their involvement (Niemietz & Tyerman, 1997, Tyerman, Niemietz & Bramley, 2002). There is no information available that we are aware of on the activation energy of CO_2 diffusion and the link to CO_2 diffusion facilitated by aquaporins, so we examined the temperature dependencies of both P_{os} and P_{CO2} to infer flow/diffusion pathways across plasma membrane vesicles derived from leaves. Inihibitors that have been reported to affect water and CO_2 transport were also examined. DIDS (4, 4'-Diisothiocyano-2, 2'-stilbenedisulfonic acid) was tested because Endeward *et al.* (2006) had shown that the apparent P_{CO2} via human AQP1 was inhibited by DIDS, meanwhile, DIDS apparently did not affect water permeability (Benga, Popescu, Pop, Hodor & Borza, 1992). We also tested the potent aquaporin inhibitor, silver sulfadiazine (AgSulf) (Niemietz & Tyerman, 2002, Yang, Kim & Verkman, 2006), to examine the pathway of CO_2 transfer. Pea plants were grown in different conditions to vary P_{os}, and CO_2 transport was measured in parallel. Here we tested the hypothesis that aquaporins are involved in CO_2 transfer and that different aquaporins and paths may be utilized by water and CO_2. Therefore it might be possible to differentially inhibit each path.

Materials and Methods

Plant material and growth conditions

Pisum sativum L cv Massey was grown in a soil mixture consisting of 1 part vermiculite perlite mix (vermiculite and perlite were mixed at a 1: 1 ratio) and 3 parts of university of California mix (UC mix) obtained from South Australian Research and Development Institute. Nutrients were supplied as mini osmocote granules (Smoult Horticultural Suppliers). The seeds were sown 4 cm deep and on a grid of 9 x 12 seeds (approx. 1 seed / cm) in trays (28 cm x 18 cm x 11 cm) with drainage holes. After sowing, approximately 1 cm of sand was spread on top of the soil to avoid insect pests. The trays were placed in a glasshouse with 12-h light/dark cycle for about 21 days and watered when required. Plants were 3 to 4 weeks old when used to isolate plasma membrane vesicles, when 20-25 leaves had emerged and were 8-10 cm high. *Arabidopsis thaliana* (Col) plants were grown in growth chamber at 21 ºC, 8 hours day-light and 50% humidity. The leaves were harvested after 8 weeks.

Stress treatments imposed

Pea plants were subjected to various types of stress before vesicle isolation. These consisted of darkness, drought and hydrogen peroxide treatments. Stomatal conductance was measured (AP4 porometer) on both control plants and stressed plants before harvesting as a measure of the degree of stress. Darkness was imposed for 46 hours, and drought was imposed for 46 h before vesicles were harvested normally near midday.

Plasma membrane vesicle isolation

Leaves (100 g) were initial homogenized in 275 mL of isolation medium (mM): 500 sucrose, 5 ascorbic acid, 1 DTT, 20 EDTA, 20 EGTA, 50 NaF, 0.5 PMSF, 0.6% (w/v) PVP, 50 HEPES-KOH pH 7.5. The homogenate was filtered in 4 layers of Miracloth (Calbiochem) and centrifuged for 10 min at 10,000 x g, then the supernatant was centrifuged for 40 min at 50,000 g to obtain microsomes. Microsomes were resuspended in (mM): 330 sucrose, 3 KCl, 0.1 EDTA, 5 K_2HPO_4/KH_2PO_4 pH 7.8. Plasma membrane vesicles (pmv) were then obtained by an aqueous two phase partitioning process (3 partitioning steps) (Larsson, Widell & Kjellbom, 1987). According to Larsson and co-workers, plant plasma membranes obtained from the upper phase (UIII) after purification by aqueous two phase partition are mainly

sealed right-side-out vesicles (Larsson, Kjellbom, Widell & Lundborg, 1984). UIII vesicles were resuspended (0.25 mL) after final centrifugation (60 min, 100,000 x g) in (mM): 330 sucrose, 0.1 EDTA, 10 Tricine-NaOH pH 7.6. These were snap frozen in liquid N_2 and stored for up to 4 weeks -80 ºC before experiments. Lowry protein assay was done to determine the total protein level of vesicles (Lowry, Rosebrough, Farr & Randall, 1951). Previous studies have demonstrated that this two-phase partitioning technique provides pure plasma membrane vesicles (Larsson, Sommarin & Widell, 1994, Larsson *et al.*, 1987, Niemietz & Tyerman, 1997). Arabidopsis vesicles were isolated following the protocol described in (Alexandersson, Saalbach, Larsson & Kjellbom, 2004).

Vesicle diameter determination

Vesicle diameter is required for calculation of osmotic water permeability and CO_2 diffusion permeability from the rate constants of the kinetics described below. It is important to measure vesicle diameter for each vesicle preparation since it may vary in response to growth conditions. Vesicle diameter was determined by dynamic laser light scattering in a NICOMP 380 particle sizer (PSS-NICOMP Particle Sizing Systems, Santa Barbara, CA, USA). The NICOMP 380 particle sizer was calibrated against latex beads of known diameter distributions. The mode was set for testing the size of vesicles. The number-weighted Gaussian distribution analysis was used to obtain the diameter of vesicles.

Western Analysis

Protein concentrations were measured using Bio-Rad Protein Assay (Biorad). A total of 7 µg protein samples were prepared by adding Bolt® LDS sample buffer (Life Technologies) and Bolt® sample reducing agent (Life Technologies) to concentrations recommended by manufacturer. Plasma membrane and tonoplast fractions were equally loaded and separated on Bolt® 4-12% Bis-Tris Plus Gel (Life Technologies,) and transferred to nitrocellulose membrane (GE Healthcare) using the Bolt® mini blot system (Life Technologies). Membranes were rinsed with T-BST buffer and blocked in 5% non-fat dried milk in T-BST for 2.5 h, followed by 4°C O/N incubation with antibodies of either the PIP1 (Vandeleur, 2009) at 1:2000, the PIP2 (Vandeleur, 2009) (1:2000), the PIP2;1 (Agrisera, 1:2000) the H^+ATPase (Agrisera, PM Marker 1:3000) or the V^+ATPase (Agrisera, TP marker; 1:2000). Following primary antibody incubations, the membranes were rinsed and incubated with anti-rabbit IgG (whole molecule)-alkaline phosphatase antibody raised in goat (Sigma-Aldrich) at

1:5000 for 2 h. All incubations were performed at room temperature unless otherwise stated. The membranes were developed using BCIP/NBT (Sigma-Aldrich) substrate and scanned membrane images were adjusted for contrast and brightness.

ELISA with PIP2;1 Antibody

The ELISA assay was performed as previously described in (Santoni, Verdoucq, Sommerer, Vinh, Pflieger & Maurel, 2006) except for the following modification: A linear detection range between fluorescence signal and protein concentrations was obtained by a 2-fold dilution series of pea vesicles of pea vesicles treated in light, dark, drought and 1-day dark treatment. Pea vesicles (6µg/mL) diluted in 50 µL PBS, pH 7.0 were coated O/N at 4 °C onto Greiner High Binding 96-well plates and blocked with 5% skim milk in PBS for 1h at 37 °C. Anti-PIP2;1 antibody (Agrisera) were used at a 1:2000 dilution and 1:5000 for goat anti-rabbit IgG (H+L)-HRP conjugate HRP. Plates were washed 3 times after each step. A concentration of 50 µM AmplexUltra Red and 1 mM hydrogen peroxide were prepared as per recommended by manufacturer's protocol (Life Technologies) and applied for 30 minutes prior to measurement with a microplate reader (POLARstar Omega, BMG Labtech).

Water permeability

The osmotic water permeability ($P_{os,}$ also referred to as P_f in other publications) (Alleva, Chara & Amodeo, 2012) was determined from the kinetics of vesicle shrinkage measured by a stopped-flow spectrofluorimeter (DX.l7MV, Applied Photophysics, Leatherhead, UK). The osmotic water permeability is proportional to membrane hydraulic conductivity and can be converted to hydraulic conductivity by multiplying P_{os} by V_w/RT, where V_w is the partial molar volume of water and R and T have the usual meanings. Note that the P_{os} does not necessarily give the same value as a diffusive water permeability (general denoted as P_d *or* P_{H2O}) especially for membranes with aquaporins present where P_{os}/P_d can be greater than one (Niemietz & Tyerman, 1997, Ye & Verkman, 1989). Further details of the method of measuring P_{os} as applied to plant plasma membrane vesicles can be found in (Niemietz & Tyerman, 1997). In the stopped-flow technique the dead time, which is the time between the end of mixing the two solutions and the beginning of observation of the reaction, was between 1-2 ms, determined according to manufacturers instructions. Light scattering (90 °) was determined with excitation at 550 nm. According to Lowry protein test, purified plasma

membrane vesicles (UIII) were diluted to 60-200 µg/ml of protein, and suspended in base solution (50 mM Mannitol, 5 mM EGTA, 50 mM HEPES-KOH, pH 7.6) and injected against a hyperosmotic solution (0.45 M extra Mannitol added to base solution) to create an inwardly directed 225 mosmol mannitol gradient after mixing 1:1.

Data was collected (7.5 kHz) and kinetics were measured for two injections at each temperature, and the average of the two was obtained. A single or double phase exponential function was fitted to the data using minimised least squares using ProData Viewer software provided by Applied Photophysics (Leatherhead, UK), and the rate constant (K_{os}) used to calculate P_{os} (van Heeswijk & van Os, 1986):

$$P_{os} = (V/A)K_{os}/(V_w C_o) \qquad \textbf{Eq 1}$$

where, V/A is the volume to surface area ratio of the vesicles, V_w is the partial molar volume of water, C_o is the external osmolarity after mixing.

The mixing chamber was surrounded by a water jacket that was connected to a water bath. The water bath regulated temperature between 13.5 °C – 22 °C as recorded in the mixing chamber. The activation energy (E_a) of vesicles shrinking was calculated using the *Arrhenius* equation: $E_a = RT(Ln(A)-Ln(K))$, where Ea is the activation energy, K is the reaction rate constant (either K_{os} or K_{CO2} described below) that depends on temperature, A is a constant, R is the universal gas constant, T is the temperature (°Kelvin).

CO_2 permeability

The membrane CO_2 diffusional permeability (P_{CO2}) was obtained from the kinetics of acidification in vesicles in response to CO_2 transport using the same stopped-flow spectrometer as described above. Vesicles were loaded with bovine carbonic anhydrase (CA) as a readily available and efficient CA in order to rapidly hydrate CO_2 to carbonic acid in the vesicles. This was done at various concentrations of CA in different experiments to examine the rate limitation of this reaction on the kinetics of vesicle acidification. The fluorescent pH-sensitive dye, HPTS (8-Hydrozy-1, 2, 6-pyrenetrisulfonate) was loaded into the vesicles to a final concentration of 0.15 mM. Further details of the technique of measuring P_{CO2} can be found in (Fang, Yang, Matthay & Verkman, 2002, Yang, Fukuda, van Hoek, Matthay, Ma & Verkman, 2000). The loading of CA and HPTS was achieved by incubating vesicles in

hypoosmotic base solution (50 mM HEPES-KOH pH 7.5) containing CA and HPTS on ice for 2 hours. Loaded vesicles were then incubated in a resealing solution (300 mM Mannitol, 50 mM HEPES-KOH, pH 7.5) on ice for 20 min. Then vesicles were quickly mixed with 5 mM quencher (p-Xylene-bis-pyridinium bromide, DPX) (Daleke, Hong & Papahadjopoulos, 1990) which quenches the fluorescence outside the vesicles.

The vesicles were injected in the stopped-flow against a CO_2 saturated resealing solution containing the same concentration of quencher. CO_2 was bubbled through resealing solution for more than 1 hour to achieve saturation. Saturation was indicated when pH reached 6.2. Kinetics of acidification were measured with an excitation wavelength of 460 nm and emission above 515 nm (OG515 long pass filter, Schott, supplied by Applied Photophysics, Leatherhead, UK). The photomultiplier voltage was normally set to 600 V, and voltage sensitivity for data acquisition of +/- 0.1 V. Data was collected (10 kHz) over a time interval from 2.0 ms to 200 ms. The fast kinetics of the decrease in fluorescence was fitted to a single exponential to obtain a rate constant, K_{CO2}. P_{CO2} was calculated as (Fang *et al.*, 2002):

$$P_{CO2}=(V/A)K_{CO2}10^{(pHf-pKa)} \qquad \textbf{Eq 2}$$

where, V/A is volume to surface area ratio, pK_a for HCO_3^- is 6.1. The final intravesicular pH (pH_f) was determined by a fluorescence ratio technique: The fluorescence of HPTS was titrated at different pH (from pH 4.0 to pH 12.0) at two different excitation wavelengths, 400 nm and 460 nm, respectively, using the stopped-flow spectrometer. The fluorescence ratios of 400 nm/460 nm at different pH were calculated and plotted against pH to make a standard ratio – pH curve. Therefore, for each measurement, the fluorescence intensities excited by each of 460 nm and 400 nm were measured, and the final pH was calculated from the standard ratio - pH curve.

Inhibitors

The aquaporin blocker silver sulfadiazine (AgSulf), and the membrane permeant CA inhibitor acetazolamide (AZ) (Hempleman, Rodriguez, Bhagat & Begay, 2000) were dissolved in 10 mM DMSO. AgSulf was used at a final concentration of 12 μM, and AZ was used at a final concentration of 50 μM. DIDS was dissolved in 75 % ethanol and a final concentration of

100 µM used. Both DMSO and ethanol at their final concentrations had no effect on kinetics of water flow or vesicle acidification. All solutions were made up fresh daily. For the vesicle shrinking experiment, vesicles (UIII) in base solution were mixed with (AgSulf), and injected against the hyperosmotic solution containing the same inhibitor concentration. For the inhibition of CO_2 uptake, vesicles were loaded with CA and HPTS in hypoosmotic base solution, then, vesicles were mixed with resealing solution. After that, vesicles were mixed with inhibitor, incubated for 10 min, and then quickly mixed with 5 mM quencher to quench the fluorescence outside the vesicles, injected against CO_2 saturated resealing solution containing the same concentration of inhibitor and quencher.

Results

Western Analysis

Western analysis of the plasma membrane vesicle (pmv) (UIII) fraction revealed minimal contamination by tonoplast membrane fractions (LIII). UIII was enriched in plasma membrane marker H^+ATPase, various PIP proteins and lacked the tonoplast V^+ATPase marker (Fig. 1).

Aquaporin protein abundance

Relative abundance of PIP2 isoforms in plasma membrane enriched vesicles isolated from pea leaves subjected to some of the treatments were indirectly measured using antibodies and fluorescence substrates. The ELISA assays showed that pmv from leaves subjected to extended dark and drought have relatively lower PIP2 protein abundance compared to two sets of control grown plants (Fig. 2). Further experiments under different growth conditions showed that relative protein abundance could decrease to 42% of controls.

Water transport across pea leaf plasma membrane vesicles

When pmv from control pea plants were subjected to a 225 mOsmol hyperosmotic gradient, light scattering rapidly increased (mean rate constant, K_{os} = 249.2 s^{-1}, SEM=14.3 s^{-1}, n= 19, 20 ^oC) indicating vesicle shrinkage (Fig. 3a). In most cases the kinetics were well fitted by a single exponential equation allowing unambiguous calculation of water permeability (P_{os} =

1331 μm s^{-1}, SEM = 107 μm s^{-1}, n=19, 20 °C). P_{os} was quite variable from one batch of plants to the next (range 579 to 2172 μm s^{-1}).

To further promote variability we subjected plants to different treatments before harvesting pmv. Stomatal conductance of control grown plants at midday ranged between 147 mmol m^{-2} s^{-1} and 340 mmol m^{-2} s^{-1} measured on five different batches. All stress treatments resulted in very low stomatal conductance: continuous darkness (46 h, 8 mmol m^{-2} s^{-1}), drought (46 h, 18 mmol m^{-2} s^{-1}), and H_2O_2 treatment (16 mmol m^{-2} s^{-1}). These treatments led to more complex vesicle shrinking kinetics which were best fit by the sum of two exponentials, but the fast phase was slower than that obtained for control plants (Fig. 3b, K_{os} = 189 s^{-1} SEM= 6 s^{-1}, n=7). This fast phase accounted for about 50% of the total change in vesicle volume and yielded a P_{os} of 991 μm s^{-1} (SEM = 58 μm s^{-1} n=7). This was significantly smaller than for control vesicles (t-test Welch corrected, P=0.01). For all treatments, after the initial water efflux, a steady final value of light-scattering was observed indicating that the vesicles were osmotically competent.

Inhibitors

In the presence of 12 μM AgSulf, the rate of shrinking decreased by over 17-fold for control pmvs (Fig. 3a dashed line) and vesicles remained osmotically competent based on the steady level of light scattering after equilibrium was achieved. For control pmvs P_{os} declined to 84 μm s^{-1} (SEM= 11 μm s^{-1} n=11). For pmvs from dark and drought treated plants, AgSulf reduced the rate of the fast phase kinetic (Fig. 3b) but had no effect on the slow phase. From the fast phase the mean P_{os} for stressed plants with AgSulf inhibition was 201 μm s^{-1} (SEM=14 μm s^{-1}, n=7, 20 °C) which is significantly larger than for control vesicles under AgSulf inhibition (t-test Welch corrected, P<0.0001). Thus there was a significantly larger effect of AgSulf on control P_{os} compared to stressed P_{os} with the overall percentage inhibition for control P_{os} of 94% compared to 80% for stressed P_{os}.

DIDS at 100 μM also strongly inhibited water transport of control plant pmv with a mean P_{os} after inhibition of 114 μm s^{-1} (SEM=30 μm s^{-1}, n=3, 20 °C) which was not significantly different from the inhibition caused by AgSulf on the same batch of vesicles.

The mean activation energy for water transport across control pea leaf pmvs was 10.8 kJ mol^{-1}. When vesicles were incubated with 12 μM AgSulf or 100 μM DIDS, the activation energy increased to 51.3 kJ mol^{-1} (Fig. 3c).

Water transport and vesicle diameter

We observed that the rate constant for shrinking (K_{os}) did not decrease with increasing vesicle diameter as would be expected based on decreasing surface area to volume ratio. If P_{os} is independent of vesicle diameter, then it would be expected that K_{os} should depend inversely on vesicle diameter with the slope proportional to the mean P_{os}. Figure 4a shows these data from across all treatments with theoretical lines for different values of P_{os} (dotted lines). There is a positive linear correlation between P_{os} and vesicle diameter (Fig. 4b). However, this might be expected for random variation in K_{os} that is unrelated to vesicle diameter since P_{os} is calculated with vesicle diameter as a factor (ie V/A = diameter/6 for a sphere). Random generation of normally distributed K_{os} with a mean and variance equal to our samples and then calculating P_{os} for each set of random values with our measured vesicle diameters gave similar correlations ($R^2 \geq 0.47$) between P_{os} and diameter in 40% of the cases (Fig. S1a). Thus the correlation obtained between P_{os} and diameter could be obtained purely by chance with random variation in K_{os}. Interestingly, with AgSulf inhibition, the linear regression of P_{os} versus vesicle diameter was not significantly different from zero ($R^2 = 0.02$, P=0.62, Fig. 4b), suggesting that there is a greater degree of inhibition of water permeability for vesicles with larger diameters. The chance of randomly obtaining an R^2 of less than 0.2 between P_{os} and vesicle diameter is about 0.05 (Fig. S1a).

There was no significant difference in vesicle diameters between stress treatments and controls; control pmvs had a diameter of 178 nm (SEM=10 nm, n= 19) while stress treatments had a mean diameter of 173.0 nm (SEM = 5 nm, n=7). However the resultant P_{os} from the fast phase for stressed plants was significantly lower than that for control plants as detailed above.

CO_2 transport into pea leaf pmvs.

Membrane CO_2 diffusion was examined in parallel with P_{os} determinations on each batch of pea leaf pmv. Uptake of CO_2 resulted in an intravesicular acidification and consequently a decrease in fluorescence as signaled by HPTS (Fig. 5a). In the case shown in Fig. 5a, the intravesicular solution contained 6 mg ml^{-1} carbonic anhydrase (CA) and the single exponential kinetics recorded at 13.5 ℃ gave a rate constant of 522.7 s^{-1}. These fast kinetics mean that the dead time of the instrument (approximately 2 ms) encroaches significantly on the amount of change observable, i.e. about 50% of the predicted change in fluorescence. The

411 extrapolated fit to time zero represents the span of the fitted acidification curve. When the CA
412 inhibitor acetazolamide (50 μM) was added to the suspension, there was a large decrease in
413 the rate constant to 75 s^{-1} (Fig. 5b). The fitted spans for control experiments at lower
414 temperatures (less than 20 ºC) were similar to the actual amplitudes obtained when AZ was
415 present (Fig. 5c). This indicates that a single exponential kinetic probably best describes the
416 entire acidification process if the stopped flow instrument could record at times less than 2
417 ms.
418 To test whether the rate constant for acidification was affected by the amount of CA
419 present and its temperature dependence, vesicles were incubated with different concentrations
420 of CA (final concentration inside the vesicles: 1.5, 4.5, 6, and 7.5 mg ml^{-1}) and acidification
421 kinetics measured at different temperatures within the stopped flow apparatus. Thus the
422 acidification rates at different temperatures were compared (Fig. 6). The Arrhenius equation
423 described the temperature kinetics well, allowing an activation energy (E_A) to be determined.
424 The activation energy decreased as the CA concentration increased (52.4 to 35.9 kJ mol^{-1}).
425 The highest activation energy was recorded with 1.5 mg ml^{-1} CA (52.4 kJ mol^{-1}) which was
426 similar to the measured activation energy for CA by itself (51.5 kJ mol^{-1}). Significant
427 differences were observed between activation energies measured in the presence of 4.5 mg
428 ml^{-1} CA and 6 mg ml^{-1} CA. Activation energies and the rate constants were not significantly
429 different with 6 and 7.5 mg ml^{-1} CA (Fig. 6b). Since CA at 6 mg ml^{-1} or greater gave the
430 maximum rates and lowest activation energy, subsequent measurements were performed
431 using CA concentrations greater than 6 mg ml^{-1}.
432 Assuming that at high intravesicular CA concentrations (> 6 mg ml^{-1}), CA activity
433 was not rate limiting, then the rate constant can be used to calculate an apparent P_{CO2}. The
434 mean rate constant at 20 ºC was 640 s^{-1} (SEM=38 s^{-1}, n=19), and the calculated P_{CO2} was 79
435 μm s^{-1} (SEM=7 μm s^{-1}, n=19). There was no significant effect of stress treatments (combined)
436 on P_{CO2} (Mean = 70 μm s^{-1} SEM =3 μm s^{-1} n=7), although across all measurements there was
437 a relative large degree of variation in P_{CO2} (15.6 to 125.3 μm s^{-1} n=26).
438
439 **Carbon dioxide transport and vesicle diameter**
440 As for water transport, we observed that the rate constant for CO_2 uptake did not decrease
441 with increasing vesicle diameter. For CO_2 uptake, the relationship between the rate constant
442 and P_{CO2} also depends on the change in intravesicular pH. The magnitude of $K_{CO2} \times 10^{(pHf-pK)}$
443 should yield a positive linear relationship with the inverse of vesicle diameter if P_{CO2} is

444 constant (Fig. 7a). Clearly this was not the case. The regression line is significantly different
445 from the relationship obtained using the mean P_{CO2} for this set of data (P<0.0001). There
446 was a significant linear correlation between P_{CO2} and vesicle diameter (Fig. 7b) as already
447 seen for P_{os} (Fig 4b). As examined for water permeability, random variation in both K_{CO2} and
448 vesicle diameters would potentially give a correlation between P_{CO2} and vesicle diameter
449 similar to that observed (Fig. 7b). However, as there is another important term in the
450 calculation of P_{CO2} (i.e. $10^{(pHf-pK)}$), the chance of obtaining a significant positive slope with an
451 $R^2 > 0.4$ purely by chance between P_{CO2} and vesicle diameter is only 4.6% (Fig. S1b). Thus,
452 at the 5% significance level, the correlation between P_{CO2} and vesicle diameter is significant.
453
454 **Inhibitors**
455 Neither AgSulf nor DIDS appeared to inhibit CO_2 transport and apparent P_{CO2} were not
456 significantly different (Fig 7b). For AgSulf and DIDS, the activation energy was lower
457 compared to control but where not significantly different from control (Mean +/- SEM (n):
458 Control 29.9 +/- 7.4 kJ mol^{-1} (6), AgSulf 23.1 +/- 7.8 kJ mol^{-1} (6), DIDS 19.9 +/- 3.3 kJ
459 mol^{-1} (3)). Neither DIDS nor AgSulf affected the kinetics of CA hydration of CO_2. P_{CO2} still
460 correlated with vesicle diameter in the presence of AgSulf (Fig. 7b), unlike P_{os} (Fig. 4b).
461
462 **Arabidopsis leaf plasma membrane vesicles**
463 For plasma membrane vesicles prepared from *Arabidopsis* leaves, P_{os} was less than that from
464 pea leaves. Interestingly, the kinetics for vesicle shrinking were best fitted by a double
465 exponential, similar to that observed for dark and drought treated pea. The P_{os} calculated
466 from the fast phase was 123 μm s^{-1} (SEM 31 μm s^{-1} n=3), an order of magnitude less than P_{os}
467 for pea. In contrast, the P_{CO2} was similar to that obtained for pea leaf plasma membrane, 95
468 μm s^{-1} (SEM 13 μm s^{-1} n =3).
469
470 **The relationship between P_{CO2} and P_{os}**
471 For each vesicle preparation, water and CO_2 transport was measured in parallel allowing for
472 an examination of any correlations between them. There were 26 separate batches of pea
473 plants and pmv isolations. A positive correlation was observed between P_{CO2} and P_{os} (R^2 =
474 0.27, P=0.0068 for slope significantly greater than zero), which is to be expected given that
475 both P_{os} and P_{CO2} appeared to be positively correlated with vesicle diameter. Fig. 8a shows
476 P_{CO2} plotted against P_{os} at 20 °C for pmv from pea leaves in addition to values obtained for

AgSulf inhibition of pea pmv, and for Arabidopsis. A similar plot is shown for just pea leaf pmv at 13.5 ºC (Fig 8b). At both temperatures we observed a significant positive linear correlation between P_{CO2} and P_{os} (excluding AgSulf treatment) (Demming model regression where errors are assumed to occur equally in the ordinate and abscissa). The darkness and drought treatments are indicated by different symbols. A positive linear correlation was also observed between P_{CO2} and P_{os} for AgSulf inhibited pea leaf pmvs, but this was not significant.

Using randomly generated values for K_{os} and K_{CO2} we can examine the chances of obtaining a correlation between P_{CO2} and P_{os} purely through having the common variable of vesicle diameter in their calculation. A correlation with positive and significant slope, and with an $R^2 \geq 0.27$ (as observed), will occur by chance in 8.8% of cases with independently randomized K_{os} and K_{CO2}. (Fig. S1c)

Discussion

High water permeability of Pea leaf pmv indicated high aquaporin activity

The measured P_{os} for pea leaf pmvs of up to 2000 μm s^{-1} is amongst the highest yet recorded for plants, surpassing by more than a factor of two those previously measured on red beet storage tissue (Alleva, Niemietz, Maurel, Parisi, Tyerman & Amodeo, 2006). In the presence of the aquaporin inhibitor, AgSulf (Niemietz & Tyerman, 2002), the average rate for water transport obtained from pea plasma membrane vesicles decreased by over 17-fold but with no apparent change in membrane integrity. The E_a increased four fold in the presence of AgSulf and towards values expected for permeation solely through the lipid bilayer. This change in E_a with inhibition of water transport has previously been used to indicate involvement of aquaporins (Niemietz & Tyerman, 1997, Niemietz & Tyerman, 2000) since if the water pore was blocked the low E_a associated with water diffusion in a water filled pore would diminish. The combination of very high water permeability, low E_a, and strong inhibition with AgSulf, indicate very high activity of aquaporins in pea leaf pmvs. In contrast, Arabidopsis leaf pmvs yielded much lower P_{os} that were similar to the higher range values previously obtained on leaf protoplasts (Morillon & Chrispeels, 2001).

With dark and drought treated pea plants, P_{os} was lower than control plants and the shrinking kinetics were more complex (double exponential kinetics). An explanation for this may be heterogeneity of vesicles, either in size or permeability (Alleva, Chara, Sutka &

510 Amodeo, 2009). There was no apparent difference in the distribution of vesicle size caused
511 by the treatments, suggesting that the difference was related to vesicle populations having
512 different P_{os}. Such heterogeneity is also seen between individual leaf protoplasts (Morillon &
513 Chrispeels, 2001). Inhibiting with AgSulf decreased the fast but not the slow phase in the two
514 phase exponential kinetics. This supports the view that the kinetic heterogeneity was caused
515 by a mixture of vesicles with high or low aquaporin activity. The treatments (drought and
516 dark) reduced the amount of PIP2 aquaporins in the membrane as demonstrated by the ELISA
517 assays, however, the reduction was not sufficient to account for the variation in P_{os} indicating
518 that post-translational modifications were probably involved in a population of cells or
519 membrane sites that then go on to form a large population of the vesicles. The degree of
520 inhibition by AgSulf was reduced on pmv isolated from stressed plants, indicating reduced
521 aquaporin activity and/or density in these plants.
522 We observed a significant positive correlation between P_{os} and vesicle diameter.
523 Vesicle diameter is used to calculate P_{os} and the correlation could reflect this as it can be
524 simulated by randomly varying K_{os}. However, with AgSulf inhibition there was no
525 correlation between P_{os} and diameter and larger vesicles had a larger degree of inhibition with
526 AgSulf than smaller vesicles. Therefore it would appear that larger vesicles display an
527 elevated P_{os} because of high aquaporin activity. One possible explanation for this is that
528 larger vesicles are stabilised by higher aquaporin activity. The effect of diameter was
529 unrelated to stress treatments since vesicle diameters were not significantly different to that of
530 controls.
531
532 **Characteristics of CO_2 transport**
533 Pea and Arabidopsis leaf pmv have P_{CO2} in the upper range of previously measured values for
534 biological membranes and is similar to that reported for Tobacco leaf plasma membrane
535 (Uehlein *et al.*, 2008b). Assuming we have accurately measured P_{CO2} relatively free of
536 unstirred layer effects (see below) and rate limitation by CA, then it would indicate that even
537 with very high aquaporin activity in a plant leaf plasma membrane this does not necessarily
538 result in a very high P_{CO2}. Interestingly, lower values of P_{os} observed for Arabidopsis leaf
539 pmv do not translate to even lower P_{CO2}, since the P_{CO2} for Arabidopsis was similar to the
540 values obtained for pea.
541 Our estimates of P_{CO2} for pea leaf pmv and those estimates made by other studies are
542 very low compared to those measured and predicted for pure lipid bilayers (Missner, Kuegler,

543 Saparov, Sommer, Mathai, Zeidel & Pohl, 2008, Missner & Pohl, 2009), this is despite the
544 extremely high values measured for P_{os} in plant membranes. Based on previous
545 measurements of ammonia permeability for a plant membrane (peribacteroid membrane,
546 PBM) of 85 μm s^{-1} (Niemietz & Tyerman, 2000) and the ratio of partition coefficients, it
547 would be expected that according to the Myer-Overton rule for lipid permeation, the P_{CO2}
548 would be 750-fold higher than the ammonia permeability (Missner & Pohl, 2009). This is
549 clearly not the case for pea leaf pmv, which gave P_{CO2} values similar to ammonia
550 permeability of the PBM. Low P_{CO2} (0.01 cm s^{-1}) has also been measured for animal cell
551 membranes and phospholipid vesicles with similar amounts of cholesterol (Itel, Al-Samir,
552 Oberg, Chami, Kumar, Supuran, Deen, Meier, Hedfalk, Gros & Endeward, 2012). In contrast
553 to water transport, P_{CO2} was not inhibited by AgSulf or DIDS. On the contrary, there was
554 generally a slight increase in P_{CO2} and lowering of the activation energy, indicative of a
555 change in the properties of the CO_2 diffusion pathway caused by these inhibitors.
556 We observed a positive correlation between P_{CO2} and vesicle diameter, similar to that
557 found for P_{os}. However, as the chance of this happening for P_{CO2} purely from random
558 variation in K_{CO2} are relatively small (4.9%), this suggests a real effect of vesicle diameter.
559 Importantly, this relationship is opposite to what might be expected if unstirred layers were
560 rate limiting. Larger vesicles would be expected to have thicker internal and external
561 unstirred layers (roughly proportional to the diameter of the vesicle) that would reduce
562 apparent P_{CO2}. This is discussed further below.
563
564
565 **Are we measuring the true membrane P_{CO2}?**
566 It is possible that the true membrane permeability to CO_2 was not measured and may reflect
567 inability to resolve fast kinetics with the instrument, rate limitation caused by CA, unstirred
568 layers, or a combination of these (Boron *et al.*, 2011). In respect of the resolution of the
569 stopped-flow, the dead-time after mixing is about 2 ms so that only approximately 30% to
570 50% of the acidification process could be monitored (Fig. 3a). In the presence of
571 acetazolamide, a CA inhibitor, CO_2 would hydrate much slower than it is transported through
572 the membrane (Gutknecht *et al.*, 1977). Thus CO_2 hydration is the rate limiting step.
573 Consequently, the rate of acidification observed cannot be interpreted in terms of CO_2
574 diffusion. Rather, it is the CO_2 hydrolysis reaction without CA catalysis. We found that the
575 amplitude of acidification with and without (extrapolated) acetazolamide were very similar

(Fig. 3c). More than 90% of the acidification process measured in the presence of acetazolamide below 20 °C could be accounted for by the extrapolated exponential fit for the reaction in the absence of acetazolamide. The similar amplitude indicates that the extrapolated single exponential fit was accurate and can represent the real CO_2 transport rate. It suggests that the measured kinetics using stopped flow did not miss a faster phase of acidification.

Previous research on CO_2 transport in plant systems has not reported any effect of CA activity at different temperatures (Heckwolf *et al.*, 2011a, Uehlein *et al.*, 2008b, Uehlein *et al.*, 2012b). Prasad *et al.* (1998) reported the effect of CA concentration differences on the measured CO_2 permeability, however, they did not explore the consequence of temperature on CA activity (Prasad, Coury, Finn & Zeidel, 1998). Here it is shown that CA concentration and changing the reaction temperature can both significantly affect the apparent P_{CO2}. In addition, the activation energy for acidification decreases with increasing CA concentration. No significant difference in the rate of acidification or activation energy was observed for intra-vesicular concentrations of CA above 5 mg ml^{-1}. We observed at low CA concentration the activation energy for acidification within the pmv was the same as the activation energy for CA free in solution (51.5 kJ mol^{-1}). At high CA concentration, the activation energy was significantly less (32 kJ mol^{-1}). This value is lower than would be predicted for pure lipid diffusion, but higher than E_a for CO_2 diffusion in water (18.8 kJ mol^{-1} (Jones, Walker & Langrish, 1995, Maharajh & Walkley, 1973). It is also similar to the value modeled for wheat leaves from measurements of g_m, which had the lowest activation energy from a range up to 76 kJ mol^{-1} from a variety of species (von Caemmerer & Evans, 2015). Interestingly the activation energy with DIDS inhibition (19.8 kJ mol^{-1}) was close to the free diffusion value.

The Meyer-Overton rule would predict much higher P_{CO2} than has currently been measured for biological membranes and the veracity of these low values, supposedly facilitated via aquaporins, has been challenged (Missner *et al.*, 2008, Missner & Pohl, 2009). Rapidly permeating substances could be rate-limited by unstirred layers rather than by the membrane lipid bilayer (Pohl, Saparov & Antonenko, 1998). Pohl concluded that large unstirred layers (1 μm) would rate limit CO_2 transport and may present much higher resistance than that of biological membranes. In the case of our pmv that were of the order of 100 to 250 nm in diameter, an effective unstirred layer can be calculated from the equations presented by (Endeward & Gros, 2009) of between 82 nm and 130 nm. This would give an

apparent P_{CO2} ranging from 0.13 to 0.21 cm s^{-1} (calculated as diffusion coefficient of CO_2 in water, 1.7 x 10^{-5} cm^2 s^{-1}, divided by the unstirred layer thickness), which is over 10 fold higher than our measured P_{CO2}. In our case the unstirred layers would be predicted to only reduce the apparent measured P_{CO2} by about 5%. Furthermore there was a positive correlation between P_{CO2} and vesicle diameter, which is opposite to that expected if unstirred layers were rate limiting.

Do aquaporins facilitate CO_2 transport?

We have tested the hypothesis that variation in P_{os} may be reflected by a similar variation in P_{CO2} of plasma membrane derived from leaves based on the correlation observed between leaf hydraulic conductivity and mesophyll conductance to CO_2 (Flexas *et al.*, 2013). If changes in aquaporin density or activity as a result of different growing conditions or vesicle diameters affected water permeability, there may be parallel changes in CO_2 permeability. Firstly however, it should be noted that the P_{CO2} we measure is a diffusional permeability, which is not directly comparable to the osmotic water permeability (P_{os}). P_{os} measures the bulk water flow in response to an osmotic gradient compared with a diffusional permeability for water movement purely by diffusion under isotonic conditions, more comparable to the P_{CO2}. When aquaporins are present and active the P_{os} can be much larger than the diffusional permeability, and previous measurements of higher plant membranes gave values of P_{os} 3 to 7-fold higher than the diffusional permeability (Niemietz & Tyerman, 1997). Thus in the case of Arabidopsis where the magnitudes of P_{os} and P_{CO2} were similar, it may be presumed that P_{CO2} is actually higher than the diffusional water permeability. For pea leaf pmv, due to the greater aquaporin activity, it may be the case that the P_{os} is much greater (more than 7 fold) than the diffusional permeability of water such that the diffusional permeabilities of CO_2 and water may be comparable.

We have observed a positive significant correlation between P_{CO2} and P_{os} for Pea leaf pmv at both high and low temperature (excluding inhibitor treatments), albeit with variation in P_{os} explaining only 27% of the variation in P_{CO2}. While vesicle diameter is a common factor in the calculation of both permeabilities, the chance of obtaining a relationship similar to the one observed from random variation in both K_{os} and K_{CO2} and using the common factor of vesicle diameter is about 9%. We contend that this is not simply a common variable phenomenon in the calculation of P_{os} and P_{CO2}. The impact of stress treatments (darkness and drought) in determining the correlation between P_{CO2} and P_{os} appears to be secondary to the

642 impact of variation in vesicle diameter between preparations, which was not affected by
643 stress treatments. Assuming that variation in aquaporin activity accounts for the variation in
644 P_{os} then at 20 ºC the correlation would indicate that aquaporins could almost double P_{CO2}
645 when at their maximum activity/density in pea leaves. However, there are many reasons why
646 a correlation between P_{os} and P_{CO2} should not occur, the main one being that not all PIP
647 aquaporins can facilitate CO_2 diffusion and furthermore those that do are not always highly
648 permeable to water (Heckwolf *et al.*, 2011a). There is one recent exception, that of AtPIP2;1,
649 which is highly expressed in Arabidopsis and shows both high water permeability and CO_2
650 permeability (Grondin *et al.*, 2015, Wang *et al.*, 2016). This aquaporin was also recently
651 shown to induce a sodium ion conductance that was abolished by co-expression with
652 AtPIP1;2 in Xenopus oocytes (Byrt, Zhao, Kourghi, Bose, Henderson, Qiu, Gilliham,
653 Schultz, Schwarz, Ramesh, Yool & Tyerman, 2016). The tetramer organization of the
654 aquaporins appears to influence CO_2 permeation and ion permeation in an opposite manner to
655 that of water permeation adding another degree of complexity. Thus the correlation we
656 observed in pea leaf plasma membrane vesicles, assumed largely derived from the leaf
657 mesophyll cells, is more likely to be indicative a controlled and correlated expression of both
658 water permeable and CO_2 permeable aquaporins.
659 The correlation between P_{CO2} and P_{os} fails when chemically inhibited values are
660 considered. Despite a large inhibition of P_{os} by AgSulf and DIDS this did not result in
661 inhibition of P_{CO2}, yet a (non-significant) correlation was still apparent between P_{CO2} and P_{os}
662 for inhibited vesicles. This could indicate that blockage of the water pathway does not
663 impact on the pathway of CO_2 diffusion. In contrast the ammonia permeability of PBM was
664 inhibited by mercury and E_a increased (Niemietz & Tyerman, 2000). Interestingly the E_a for
665 CO_2 transport tended to decline with DIDS and AgSulf. One hypothesis that may explain
666 these results is that CO_2 may move via the central pore of the aquaporin tetramer and that
667 these inhibitors lead to a change in structure of the central cavity of the tetramer to affect CO_2
668 diffusion. Hub *et al.* (2006, 2008) used atomic molecular dynamics simulations to address
669 the pathway of CO_2 transport through AQP1. According to their calculation, the free energy
670 barrier for CO_2 permeation through an empty central cavity is significantly smaller than for
671 the monomeric channel. They concluded that significant aquaporin-1-mediated
672 CO_2 permeation is to be expected only in membranes with a low intrinsic CO_2 permeability
673 (Hub & de Groot, 2006, Hub & De Groot, 2008). Since DIDS inhibited the CO_2 pathway of
674 HsAQP1 by half, it possibly interferes with the central pore of HsAQP1 (Endeward, Musa-

675 Aziz, Cooper, Chen, Pelletier, Virkki, Supuran, King, Boron & Gros, 2006). However, for
676 pea leaf aquaporins, DIDS did not inhibit P_{CO2} but did inhibit P_{os}. Apparently DIDS does not
677 work in the same way for pea leaf aquaporins as it does in HsAQP1. A CO_2 pathway through
678 plant aquaporin tetramers independent of the monomer water pore was also suggested for
679 tobacco NtAQP1 based on the changes in P_{CO2} with different ratios of NtAQP1 (CO_2
680 permeable) and NtPIP2;1 (water permeable but not CO_2 permeable) co-expressed in yeast
681 (Otto *et al.*, 2010).
682 Molecular and biophysical evidence has accumulated that aquaporins can facilitate the
683 diffusion of CO_2 across membranes (Heckwolf *et al.*, 2011a, Katsuhara, Hanba, Shibasaka,
684 Hayashi, Hayakawa & Kasamo, 2003, Musa-Aziz, Chen, Pelletier & Boron, 2009, Nakhoul,
685 Davis, Romero & Boron, 1998, Otto *et al.*, 2010, Terashima & Ono, 2002a, Uehlein *et al.*,
686 2012b). Within plant membranes, (Uehlein *et al.*, 2003a) demonstrated that tobacco plasma
687 membrane aquaporin NtAQP1 may facilitate CO_2 transport as well as its established role as a
688 water channel. The over-expression of NtAQP1 heightens membrane permeability for both
689 water and CO_2, and increases leaf growth. The *Arabidopsis thaliana* aquaporin AtPIP1;2 is
690 also indicated as a CO_2 transport facilitator (Heckwolf *et al.*, 2011a). Uehlein *et al.* (2012)
691 studied the CO_2 flux into *Arabidopsis* mesophyll cells by using a scanning pH microelectrode
692 and they suggested that cellular CO_2 transport was not limited by unstirred layers but rather
693 depended on the expression of AtPIP1;2. Further direct support for involvement of
694 aquaporins comes from the incorporation of AtPIP1;2 into artificial membranes that have
695 very low CO_2 permeability (Uehlein, Otto, Eilingsfeld, Itel, Meier & Kaldenhoff, 2012a).
696
697 **Overlap between water and CO_2 diffusion pathways**
698 CO_2 and water share a common diffusion path between the atmosphere and the mesophyll
699 apoplast, although the relative fluxes at the cell surfaces are likely to vary considerably. The
700 relative importance of apoplastic versus symplastic pathways of water movement for
701 transpiration from xylem to mesophyll cell wall surfaces is not known. If the symplastic path
702 dominated, then water flow across the mesophyll plasma membrane would overlap with CO_2
703 exchange. If plasma membrane P_{CO2} was strongly influenced by aquaporins, then it is
704 possible that it could interact with P_{os}. By comparing different pmv preparations, it was
705 shown that P_{CO2} covaried with P_{os} (Fig. 8). However, as the relative balance between the two
706 permeabilities was clearly different for pea and Arabidopsis, water and CO_2 follow different
707 pathways. This is consistent with specialized functions for the different aquaporins, or

utilizing different parts of the protein for the transfer e.g. central pore of a monomer for water and the external channel formed between aquaporin tetramers for CO_2 (Otto *et al.*, 2010). At the leaf level, it has been shown that leaf hydraulic conductance correlates with mesophyll conductance across species (Flexas *et al.*, 2013). This coordination could indicate that aquaporins comprise a major part of the total resistance for each parameter,

Supplementary Material

Figure S1 Probability densities of R^2 for correlations between P_{os} and vesicle diameter, P_{CO2} and vesicle diameter, and P_{CO2} versus P_{os} with random variation in rate constants.

Acknowledgements

Thanks to Wendy Sullivan for expert technical assistance. Stephanie McCaffery for her expertise in preparing membranes, having to spend long periods in the cold room despite an aversion to low temperatures. This research was supported by The Australian Research Council (ARC) Centre of Excellence in Plant Energy Biology (CE140100008), DP0771413, and ARC COE for Translational photosynthesis (CE140100015).

Literature Cited

Alexandersson E., Saalbach G., Larsson C. & Kjellbom P. (2004) Arabidopsis plasma membrane proteomics identifies components of transport, signal transduction and membrane trafficking. *Plant and Cell Physiology*, **45**, 1543-1556.

Alleva K., Chara O. & Amodeo G. (2012) Aquaporins: Another piece in the osmotic puzzle. *Febs Letters*, **586**, 2991-2999.

Alleva K., Chara O., Sutka M.R. & Amodeo G. (2009) Analysis of the source of heterogeneity in the osmotic response of plant membrane vesicles. *European Biophysics Journal*, **38**, 175-184.

Alleva K., Niemietz C.M., Maurel C., Parisi M., Tyerman S.D. & Amodeo G. (2006) Plasma membrane of Beta vulgaris storage root shows high water channel activity regulated by cytoplasmic pH and a dual range of calcium concentrations. *Journal of Experimental Botany*, **57**, 609-621.

Benga G., Popescu O., Pop V.I., Hodor P. & Borza T. (1992) EFFECTS ON WATER DIFFUSION OF INHIBITORS AFFECTING VARIOUS TRANSPORT PROCESSES IN HUMAN RED-BLOOD-CELLS. *European Journal of Cell Biology*, **59**, 219-223.

Bertl A. & Kaldenhoff R. (2007) Function of a separate NH(3)-pore in Aquaporin TIP2;2 from wheat. *FEBS Lett.*, **581**, 5413-5417.

Boron W.F. (2010) Sharpey-Schafer lecture: gas channels. *Exp Physiol*, **95**, 1107-1130.

Boron W.F., Endeward V., Gros G., Musa-Aziz R. & Pohl P. (2011) Intrinsic CO2 Permeability of Cell Membranes and Potential Biological Relevance of CO2 Channels. *ChemPhysChem*, **12**, 1017-1019.

Byrt C.S., Zhao M., Kourghi M., Bose J., Henderson S.W., Qiu J., Gilliham M., Schultz C., Schwarz M., Ramesh S.A., Yool A. & Tyerman S.D. (2016) Non-selective cation channel activity of aquaporin AtPIP2;1 regulated by Ca2+ and pH. *Plant Cell and Environment*, **Submitted**.

Daleke D.L., Hong K. & Papahadjopoulos D. (1990) Endocytosis of liposomes by macrophages: binding, acidification and leakage of liposomes monitored by a new fluorescence assay. *Biochimica et Biophysica Acta (BBA) - Biomembranes*, **1024**, 352-366.

Endeward V., Al-Samir S., Itel F. & Gros G. (2014) How does carbon dioxide permeate cell membranes? A discussion of concepts, results and methods. *Frontiers in Physiology*, **4**, 21.

Endeward V. & Gros G. (2005) Low carbon dioxide permeability of the apical epithelial membrane of guinea-pig colon. *The Journal of Physiology*, **567**, 253-265.

Endeward V. & Gros G. (2009) Extra- and intracellular unstirred layer effects in measurements of CO2 diffusion across membranes - a novel approach applied to the mass spectrometric O-18 technique for red blood cells. *Journal of Physiology-London*, **587**, 1153-1167.

Endeward V., Musa-Aziz R., Cooper G.J., Chen L.-M., Pelletier M.F., Virkki L.V., Supuran C.T., King L.S., Boron W.F. & Gros G. (2006) Evidence that aquaporin 1 is a major pathway for CO2 transport across the human erythrocyte membrane. *The FASEB Journal*, **20**, 1974-1981.

Evans J.R. (1999) Leaf anatomy enables more equal access to light and CO2 between chloroplasts. *New Phytologist*, **143**, 93-104.

Evans J.R., Kaldenhoff R., Genty B. & Terashima I. (2009) Resistances along the CO2 diffusion pathway inside leaves. *Journal of Experimental Botany*, **60**, 2235-2248.

Fang X., Yang B., Matthay M.A. & Verkman A.S. (2002) Evidence against aquaporin-1-dependent CO2 permeability in lung and kidney. *The Journal of Physiology*, **542**, 63-69.

Flexas J., Barbour M.M., Brendel O., Cabrera H.M., Carriqui M., Diaz-Espejo A., Douthe C., Dreyer E., Ferrio J.P., Gago J., Galle A., Galmes J., Kodama N., Medrano H., Niinemets U., Peguero-Pina J.J., Pou A., Ribas-Carbo M., Tomas M., Tosens T. & Warren C.R. (2012) Mesophyll diffusion conductance to CO2: An unappreciated central player in photosynthesis. *Plant Science*, **193**, 70-84.

Flexas J. & Diaz-Espejo A. (2015) Interspecific differences in temperature response of mesophyll conductance: food for thought on its origin and regulation. *Plant Cell and Environment*, **38**, 625-628.

Flexas J., Scoffoni C., Gago J. & Sack L. (2013) Leaf mesophyll conductance and leaf hydraulic conductance: an introduction to their measurement and coordination. *Journal of Experimental Botany*, **64**, 3965-3981.

Grondin A., Rodrigues O., Verdoucq L., Merlot S., Leonhardt N. & Maurel C. (2015) Aquaporins Contribute to ABA-Triggered Stomatal Closure through OST1-Mediated Phosphorylation. *Plant Cell*, **27**, 1945-1954.

Gutknecht J., Bisson M.A. & Tosteson F.C. (1977) DIFFUSION OF CARBON-DIOXIDE THROUGH LIPID BILAYER MEMBRANES - EFFECTS OF CARBONIC-ANHYDRASE, BICARBONATE, AND UNSTIRRED LAYERS. *Journal of General Physiology*, **69**, 779-794.

Heckwolf M., Pater D., Hanson D.T. & Kaldenhoff R. (2011a) The Arabidopsis thaliana aquaporin AtPIP1;2 is a physiologically relevant CO2 transport facilitator. *The Plant Journal*, **67**, 795-804.

Heckwolf M., Pater D., Hanson D.T. & Kaldenhoff R. (2011b) The Arabidopsis thaliana aquaporin AtPIP1;2 is a physiologically relevant CO(2) transport facilitator. *The Plant journal : for cell and molecular biology*, **67**, 795-804.

Heinen R.B., Bienert G.P., Cohen D., Chevalier A.S., Uehlein N., Hachez C., Kaldenhoff R., Le Thiec D. & Chaumont F. (2014) Expression and characterization of plasma membrane aquaporins in stomatal complexes of Zea mays. *Plant Molecular Biology*, **86**, 335-350.

Hempleman S.C., Rodriguez T.A., Bhagat Y.A. & Begay R.S. (2000) Benzolamide, acetazolamide, and signal transduction in avian intrapulmonary chemoreceptors. *American Journal of Physiology - Regulatory, Integrative and Comparative Physiology*, **279**, R1988-R1995.

Hub J.S. & de Groot B.L. (2006) Does CO2 permeate through aquaporin-1? *Biophysical Journal*, **91**, 842-848.

Hub J.S. & De Groot B.L. (2008) Mechanism of selectivity in aquaporins and aquaglyceroporins. *Proceedings of the National Academy of Sciences of the United States of America*, **105**, 1198-1203.

Itel F., Al-Samir S., Oberg F., Chami M., Kumar M., Supuran C.T., Deen P.M.T., Meier W., Hedfalk K., Gros G. & Endeward V. (2012) CO2 permeability of cell membranes is regulated by membrane cholesterol and protein gas channels. *Faseb Journal*, **26**, 5182-5191.

Jahn T.P., Moller A.L.B., Zeuthen T., Holm L.M., Klaerke D.A., Mohsin B., Kuhlbrandt W. & Schjoerring J.K. (2004) Aquaporin homologues in plants and mammals transport ammonia. *Febs Letters*, **574**, 31-36.

Jones T.G., Walker J.C.F. & Langrish T.A.G. (1995) DISSOLVED CARBON-DIOXIDE GAS-DIFFUSION IN GREEN NOTHOFAGUS-FUSCA HEARTWOOD. *Wood Science and Technology*, **29**, 171-176.

Kaldenhoff R. (2012) A Revised View on Cellular CO2 Transport Mechanisms: Biophysics, Physiology and Genomics of Aquaporin-Facilitated CO2 Transport in Plants. *Biophysical Journal*, **102**, 627a-627a.

Katsuhara M., Hanba Y., Shibasaka M., Hayashi Y., Hayakawa T. & Kasamo K. (2003) Increase in CO2 permeability (diffusion conductance) in leaves of transgenic rice plant over-expressing barley aquaporin. *Plant and Cell Physiology*, **44**, S86-S86.

Larsson C., Kjellbom P., Widell S. & Lundborg T. (1984) SIDEDNESS OF PLANT PLASMA-MEMBRANE VESICLES PURIFIED BY PARTITIONING IN AQUEOUS 2-PHASE SYSTEMS. *Febs Letters*, **171**, 271-276.

Larsson C., Sommarin M. & Widell S. (1994) [44] Isolation of highly purified plant plasma membranes and separation of inside-out and right-side-out vesicles. In: *Methods in Enzymology* (ed G.J. Harry Walter), pp. 451-469. Academic Press.

Larsson C., Widell S. & Kjellbom P. (1987) [52] Preparation of high-purity plasma membranes. In: *Methods in Enzymology* (ed R.D. Lester Packer), pp. 558-568. Academic Press.

829 Loque D., Ludewig U., Yuan L. & von Wiren N. (2005) Tonoplast Intrinsic Proteins AtTIP2;1 and
830 AtTIP2;3 Facilitate NH3 Transport into the Vacuole. *Plant Physiology*, **137**, 671-680.
831 Lowry O.H., Rosebrough N.J., Farr A.L. & Randall R.J. (1951) PROTEIN MEASUREMENT WITH
832 THE FOLIN PHENOL REAGENT. *Journal of Biological Chemistry*, **193**, 265-275.
833 Maharajh D.M. & Walkley J. (1973) TEMPERATURE-DEPENDENCE OF DIFFUSION-
834 COEFFICIENTS OF AR, CO2, CH4, CH3CL, CH3BR, AND CHCL2F IN WATER. *Canadian*
835 *Journal of Chemistry-Revue Canadienne De Chimie*, **51**, 944-952.
836 Maurel C., Boursiac Y., Luu D.T., Santoni V., Shahzad Z. & Verdoucq L. (2015) AQUAPORINS IN
837 PLANTS. *Physiological Reviews*, **95**, 1321-1358.
838 Missner A., Kuegler P., Saparov S.M., Sommer K., Mathai J.C., Zeidel M.L. & Pohl P. (2008) Carbon
839 dioxide transport through membranes. *Journal of Biological Chemistry*, **283**, 25340-
840 25347.
841 Missner A. & Pohl P. (2009) 110 Years of the Meyer–Overton Rule: Predicting Membrane
842 Permeability of Gases and Other Small Compounds. *ChemPhysChem*, **10**, 1405-1414.
843 Morillon R. & Chrispeels M.J. (2001) The role of ABA and the transpiration stream in the
844 regulation of the osmotic water permeability of leaf cells. *Proceedings of the National*
845 *Academy of Sciences of the United States of America*, **98**, 14138-14143.
846 Musa-Aziz R., Chen L.-M., Pelletier M.F. & Boron W.F. (2009) Relative CO2/NH3 selectivities of
847 AQP1, AQP4, AQP5, AmtB, and RhAG. *Proceedings of the National Academy of Sciences of*
848 *the United States of America*, **106**, 5406-5411.
849 Nakhoul N.L., Davis B.A., Romero M.F. & Boron W.F. (1998) Effect of expressing the water
850 channel aquaporin-1 on the CO2 permeability of Xenopus oocytes. *American Journal of*
851 *Physiology-Cell Physiology*, **274**, C543-C548.
852 Negrete H.O., Lavelle J.P., Berg J., Lewis S.A. & Zeidel M.L. (1996) Permeability properties of the
853 intact mammalian bladder epithelium. *American Journal of Physiology - Renal Physiology*,
854 **271**, F886-F894.
855 Niemietz C.M. & Tyerman S.D. (1997) Characterization of water channels in wheat root
856 membrane vesicles. *Plant Physiology*, **115**, 561-567.
857 Niemietz C.M. & Tyerman S.D. (2000) Channel-mediated permeation of ammonia gas through
858 the peribacteroid membrane of soybean nodules. *Febs Letters*, **465**, 110-114.
859 Niemietz C.M. & Tyerman S.D. (2002) New potent inhibitors of aquaporins: silver and gold
860 compounds inhibit aquaporins of plant and human origin. *Febs Letters*, **531**, 443-447.
861 Niinemets O. & Reichstein M. (2003) Controls on the emission of plant volatiles through stomata:
862 A sensitivity analysis. *Journal of Geophysical Research*, **108**, ACH3-1-10.
863 Otto B., Uehlein N., Sdorra S., Fischer M., Ayaz M., Belastegui-Macadam X., Heckwolf M., Lachnit
864 M., Pede N., Priem N., Reinhard A., Siegfart S., Urban M. & Kaldenhoff R. (2010)
865 Aquaporin Tetramer Composition Modifies the Function of Tobacco Aquaporins. *Journal*
866 *of Biological Chemistry*, **285**, 31253-31260.
867 Pohl P., Saparov S.M. & Antonenko Y.N. (1998) The size of the unstirred layer as a function of the
868 solute diffusion coefficient. *Biophysical Journal*, **75**, 1403-1409.
869 Postaire O., Tournaire-Roux C., Grondin A., Boursiac Y., Morillon R., Schaffner A.R. & Maurel C.
870 (2010) A PIP1 Aquaporin Contributes to Hydrostatic Pressure-Induced Water Transport
871 in Both the Root and Rosette of Arabidopsis. *Plant Physiology*, **152**, 1418-1430.
872 Prasad G.V.R., Coury L.A., Finn F. & Zeidel M.L. (1998) Reconstituted aquaporin 1 water channels
873 transport CO2 across membranes. *Journal of Biological Chemistry*, **273**, 33123-33126.
874 Santoni V., Verdoucq L., Sommerer N., Vinh J., Pflieger D. & Maurel C. (2006) Methylation of
875 aquaporins in plant plasma membrane. *Biochemical Journal*, **400**, 189-197.
876 Sommer A., Geist B., Da Ines O., Gehwolf R., Schaffner A.R. & Obermeyer G. (2008) Ectopic
877 expression of Arabidopsis thaliana plasma membrane intrinsic protein 2 aquaporins in
878 lily pollen increases the plasma membrane water permeability of grain but not of tube
879 protoplasts. *New Phytologist*, **180**, 787-797.

880 Terashima I. & Ono K. (2002a) Effects of HgCl2 on CO2 dependence of leaf photosynthesis:
881 Evidence indicating involvement of aquaporins in CO2 diffusion across the plasma
882 membrane. *Plant and Cell Physiology*, **43**, 70-78.
883 Terashima I. & Ono K. (2002b) Effects of HgCl(2) on CO(2) dependence of leaf photosynthesis:
884 evidence indicating involvement of aquaporins in CO(2) diffusion across the plasma
885 membrane. *Plant Cell Physiol*, **43**, 70-78.
886 Tyerman S.D., Niemietz C.M. & Bramley H. (2002) Plant aquaporins: multifunctional water and
887 solute channels with expanding roles. *Plant Cell and Environment*, **25**, 173-194.
888 Uehlein N., Lovisolo C., Siefritz F. & Kaldenhoff R. (2003a) The tobacco aquaporin NtAQP1 is a
889 membrane CO2 pore with physiological functions. *Nature*, **425**, 734-737.
890 Uehlein N., Lovisolo C., Siefritz F. & Kaldenhoff R. (2003b) The tobacco aquaporin NtAQP1 is a
891 membrane CO2 pore with physiological functions. *Nature*, **425**, 734-737.
892 Uehlein N., Otto B., Eilingsfeld A., Itel F., Meier W. & Kaldenhoff R. (2012a) Gas-tight triblock-
893 copolymer membranes are converted to CO2 permeable by insertion of plant
894 aquaporins. *Scientific Reports*, **2**.
895 Uehlein N., Otto B., Hanson D.T., Fischer M., McDowell N. & Kaldenhoff R. (2008a) Function of
896 Nicotiana tabacum aquaporins as chloroplast gas pores challenges the concept of
897 membrane CO2 permeability. *Plant Cell*, **20**, 648-657.
898 Uehlein N., Otto B., Hanson D.T., Fischer M., McDowell N. & Kaldenhoff R. (2008b) Function of
899 Nicotiana tabacum Aquaporins as Chloroplast Gas Pores Challenges the Concept of
900 Membrane CO2 Permeability. *The Plant Cell Online*, **20**, 648-657.
901 Uehlein N., Sperling H., Heckwolf M. & Kaldenhoff R. (2012b) The Arabidopsis aquaporin PIP1;2
902 rules cellular CO2 uptake. *Plant Cell and Environment*, **35**, 1077-1083.
903 van Heeswijk M.P.E. & van Os C.H. (1986) Osmotic water permeabilities of brush border and
904 basolateral membrane vesicles from rat renal cortex and small intestine. *Journal of*
905 *Membrane Biology*, **92**, 183-193.
906 von Caemmerer S. & Evans J.R. (2015) Temperature responses of mesophyll conductance differ
907 greatly between species. *Plant Cell and Environment*, **38**, 629-637.
908 Waisbren S.J., Geibel J.P., Modlin I.M. & Boron W.F. (1994) Unusual permeability properties of
909 gastric gland cells. *Nature*, **368**, 332-335.
910 Wang C., Hu H., Qin X., Zeise B., Xu D., Rappel W.-J., Boron W.F. & Schroeder J.I. (2016)
911 Reconstitution of CO2 regulation of SLAC1 anion channel and function of CO2-
912 permeable PIP2;1 aquaporin as carbonic anhydrase 4 interactor. *The Plant Cell*.
913 Warren C.R. (2008) Stand aside stomata, another actor deserves centre stage: the forgotten role
914 of the internal conductance to CO(2) transfer. *Journal of Experimental Botany*, **59**, 1475-
915 1487.
916 Yang B.X., Fukuda N., van Hoek A., Matthay M.A., Ma T.H. & Verkman A.S. (2000) Carbon dioxide
917 permeability of aquaporin-1 measured in erythrocytes and lung of aquaporin-1 null
918 mice and in reconstituted proteoliposomes. *Journal of Biological Chemistry*, **275**, 2686-
919 2692.
920 Yang B.X., Kim J.K. & Verkman A.S. (2006) Comparative efficacy of HgCl2 with candidate
921 aquaporin-1 inhibitors DMSO, gold, TEA(+) and acetazolamide. *Febs Letters*, **580**, 6679-
922 6684.
923 Ye R.G. & Verkman A.S. (1989) SIMULTANEOUS OPTICAL MEASUREMENT OF OSMOTIC AND
924 DIFFUSIONAL WATER PERMEABILITY IN CELLS AND LIPOSOMES. *Biochemistry*, **28**,
925 824-829.
926
927

928 **Figure Legends**

929

930 **Figure 1.** Coomassie Blue Stain and Western blot analysis with (A) H^+ATPase, (B)
931 V^+ATPase and (C) PIP1, PIP2 and PIP 2;1 antibodies following separation of plasma
932 membrane enriched fraction (UIII) and tonoplast fraction (LIII) on SDS-Page.

933

934 **Figure 2**. Drought and dark treatments reduced the relative abundance of PIP2 proteins in
935 leaf plasma membrane vesicles. Relative abundance from ELISA analysis of PIP2 protein at
936 constant total protein (6.25 μg) abundance in plasma membrane vesicles from controls and
937 treatments used on pea. Mean +/- SEM of triplicate measurements.

938

939 **Figure 3.** Water transport properties for plasma membrane vesicles from control and drought
940 treated pea plants and the effect of AgSulf. (a) Example kinetics (20 °C) of control grown pea
941 plants. Black continuous line: vesicle shrinking of pea leaf pmvs subjected to an osmotic
942 gradient of 225 mOsmol. Grey line: effect of AgSulf (12 μM) on the kinetics. (b) Example
943 kinetics from drought treated pea plants and the effect of AgSulf, details as in (a). (c)
944 Temperature dependence of shrinking kinetics without (filled circles) and with (filled squares)
945 AgSulf or DIDS (open circles) for control plants. Shrinking rates were obtained for
946 temperatures ranging from 13.5 to 22 °C. Error bars are SEM (N=7) for control and AgSulf
947 and for DIDS (N=3).

948

949 **Figure 4.** Effect of pea leaf vesicle diameter on K_{os} and P_{os}. (a) K_{os} is plotted against the
950 inverse of vesicle diameter since according to Eq 1 if P_{os} is constant there should be a
951 positive linear association between K_{os} and 1/diameter. These are shown for different values
952 of P_{os} (dotted lines). A linear fit to the data is also shown (+/- 95% confidence interval)
953 which is significantly different to that which would be obtained using the average P_{os}. (b) P_{os}
954 as a function of vesicle diameter for all batches of pea leaf pmv (solid circles) and for those
955 treated with AgSulf (open circles). The coefficients of the linear regression for the
956 uninhibited pmv were: $R^2 = 0.48$; slope = 7.8 μm s^{-1} nm^{-1} (95% confidence = 4.4 to 11.17 μm
957 s^{-1} nm^{-1}); intercept = -155 μm s^{-1} (95% confidence = -760 to 449 μm s^{-1}), and AgSulf
958 inhibited pmv $R^2 = 0.02$; slope = 0.2 μm s^{-1} nm^{-1} (95% confidence = -0.7 to 1.2 μm s^{-1} nm^{-1});
959 intercept = 90 μm s^{-1} (95% confidence = -90 to 271 μm s^{-1}).

960

961

962 **Figure 5**. Time course of acidification in vesicles in response to CO_2 transport with and
963 without acetazolamide at 13.5 ℃. (a) Time course of acidification in plasma membrane
964 vesicles in response to CO_2 transport. The exponential fit is indicated by the dotted line. (b)
965 With 50 μM acetazolamide (note change in time scale). (c) Comparison of the amplitude of
966 the change in acidification in the presence or absence of acetazolamide at different
967 temperatures. Mean +/- SEM (N=3).

968

969 **Figure 6.** Temperature dependence of CO_2 acidification kinetics for pea leaf pmv and the
970 effect of carbonic anhydrase (CA). (a) Arrhenius plots (13.5 ℃ to 23 ℃) of the rate of
971 acidification at different intra-vesicular CA concentrations (solid circles 1.5 mg/ml; open
972 circles 4.5 mg/ml; solid squares 6 mg/ml; solid triangles 7.5 mg/ml)). (b) Activation energy
973 from the fits in (a) plotted against the intra-vesicular concentration of CA. Different letters
974 indicate significant differences ($P < 0.05$). Mean +/- SEM (N=4).

975

976 **Figure 7.** Effect of pea leaf vesicle diameter on K_{CO2} and P_{CO2}. (a) K_{CO2} x $10^{(pHf - pK)}$ is
977 plotted against the inverse of vesicle diameter since according to Eq 2 if P_{CO2} is constant
978 there should be a positive linear association between K_{CO2} x $10^{(pHf - pK)}$ and 1/diameter. These
979 are shown for different values of P_{CO2} (dotted lines). A linear fit to the data is also shown
980 (+/- 95% confidence interval) which is significantly different to that which would be obtained
981 using the average P_{CO2}. (b) P_{CO2} as a function of vesicle diameter for all batches of pea leaf
982 pmv (solid circles) and for those treated with AgSulf (open circles). The coefficients of the
983 linear regression for the uninhibited pmvs were: $R^2 = 0.40$; slope = 0.41 μm s^{-1} nm^{-1} (95%
984 confidence = 0.19 to 0.61 μm s^{-1} nm^{-1}); intercept = 4.5 μm s^{-1} (95% confidence = -33 to 42
985 μm s^{-1}), and AgSulf inhibited pmvs $R^2 = 0.61$; slope = 0.46 μm s^{-1} nm^{-1} (95% confidence =
986 0.09 to 0.82 μm s^{-1} nm^{-1}); intercept = -1.9 μm s^{-1} (95% confidence = -73 to 69 μm s^{-1}).

987

988

989 **Figure 8.** Relationship between P_{CO2} and P_{os} measured on the same batches of vesicles at 20
990 ºC (a) and 13.5 ºC (b). Some batches of plants were treated with darkness and drought as
991 indicated by different symbols in (a). Also shown are the AgSulf treated pmv and
992 *Arabidopsis* leaf pmv. The linear regression coefficients are: (a) Uninhibited 20 ºC, R^2 =
993 0.27, slope = 0.03 (95% confidence = 0.009 to 0.05), intercept 38.6 μm s^{-1} (95% confidence

994 = 10.9 to 66.2 μm s^{-1}); AgSulf inhibited 20 °C, R^2 = 0.18, slope = 0.32 (95% confidence = -
995 0.35 to 0.99), intercept 58.8 μm s^{-1} (95% confidence = -3.3 to 120.8 μm s^{-1}) (b) 13.5 °C, R^2 =
996 0.25, slope = 0.04 (95% confidence = 0.002 to 0.08), intercept 10.5 μm s^{-1} (95% confidence
997 = -39.9 to 60.9 μm s^{-1}.
998

Figures

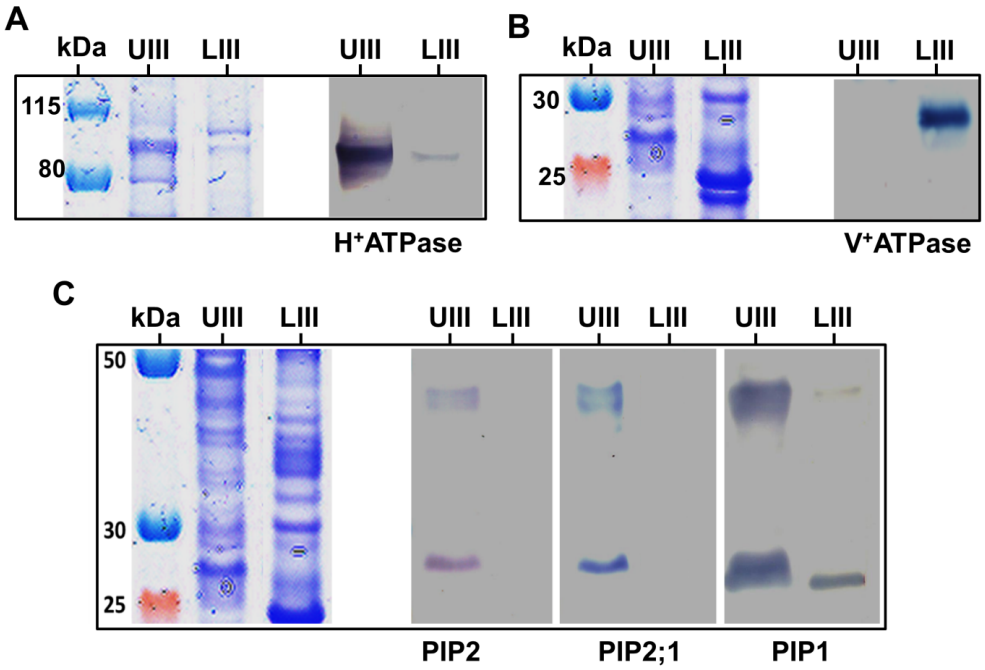

Figure 1. Coomassie Blue Stain and Western blot analysis with (A) H^+ATPase, (B) V^+ATPase and (C) PIP1, PIP2 and PIP 2;1 antibodies following separation of plasma membrane enriched fraction (UIII) and tonoplast fraction (LIII) on SDS-Page.

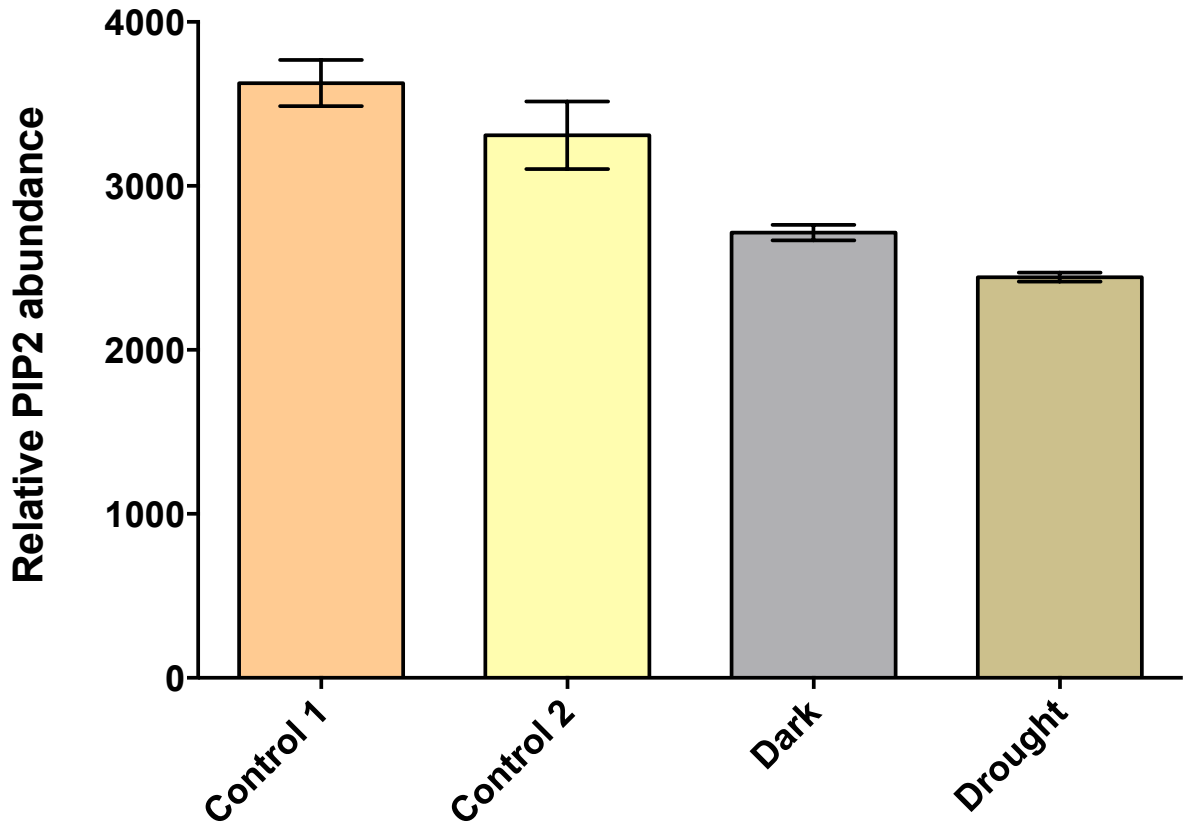

Figure 2. Drought and dark treatments reduced the relative abundance of PIP2 proteins in leaf plasma membrane vesicles used in the stopped flow experiments. Relative abundance from ELISA analysis of PIP2 protein at constant total protein (6.25 µg) abundance in plasma membrane vesicles from controls (two sets) and treatments used on pea. Mean +/- SEM of triplicate measurements.

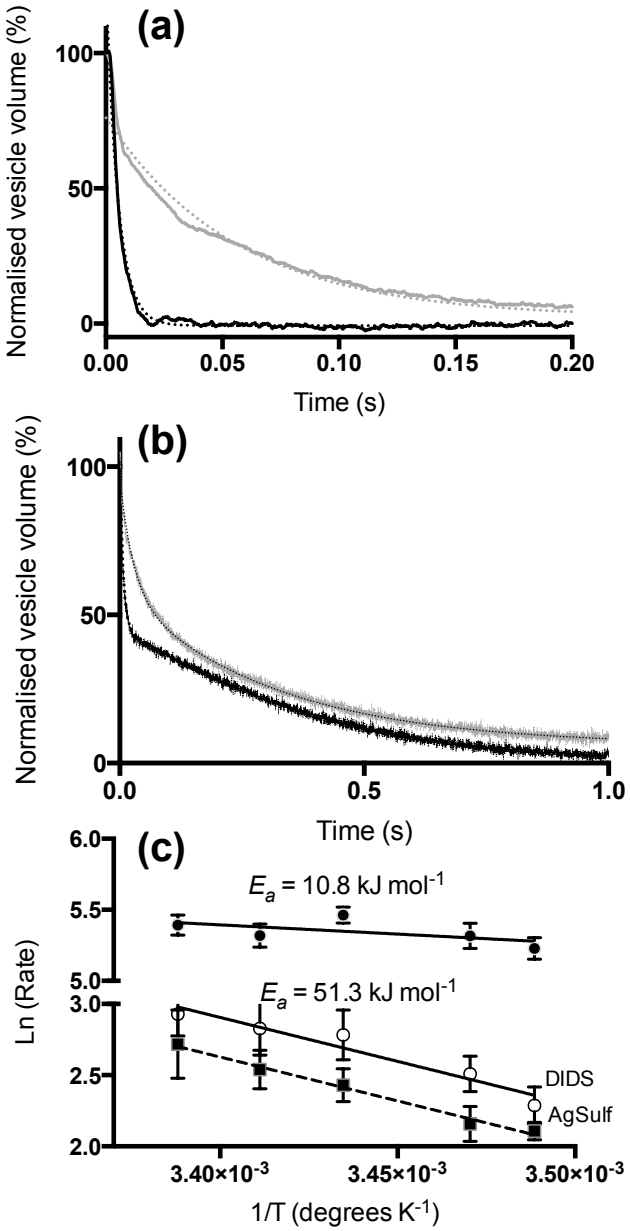

Figure 3. Water transport properties for plasma membrane vesicles from control and drought treated pea plants and the effect of AgSulf. (a) Example kinetics (20 ºC) of control grown pea plants. Black continuous line: vesicle shrinking of pea leaf pmv subjected to an osmotic gradient of 225 mOsmol. Grey line: effect of AgSulf (12 µM) on the kinetics. (b) Example kinetics from drought treated pea plants and the effect of AgSulf, details as in (a). Dotted lines in (a) and (b) indicate fitted exponentials. (c) Temperature dependence of shrinking kinetics without (filled circles) and with (filled squares) AgSulf or DIDS (open circles) for control plants. Shrinking rates were obtained for temperatures ranging from 13.5 to 22 ºC Mean +/- SEM (N=7) for control and AgSulf and DIDS (N=3).

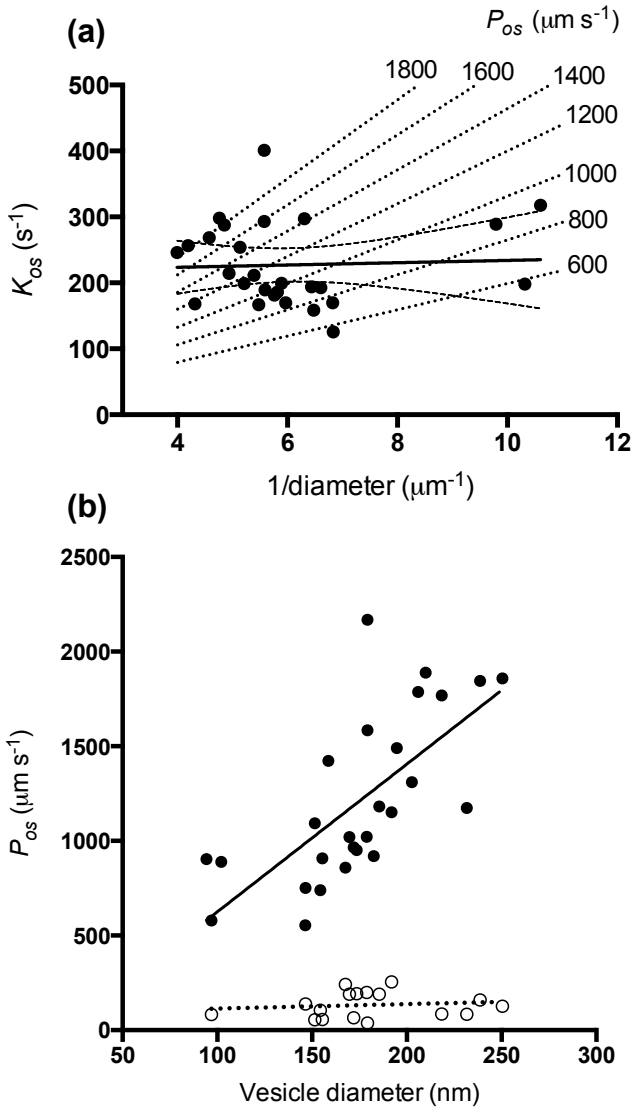

Figure 4. Effect of pea leaf vesicle diameter on K_{os} and P_{os}. (a) K_{os} is plotted against the inverse of vesicle diameter since according to Eq 1 if P_{os} is constant there should be a positive linear association between K_{os} and 1/diameter. These are shown for different values of P_{os} (dotted lines). A linear fit to the data is also shown (+/- 95% confidence interval) which is significantly different to that which would be obtained using the average P_{os}. (b) P_{os} as a function of vesicle diameter for all batches of pea leaf pmv (solid circles) and for those treated with AgSulf (open circles). The coefficients of the linear regression for the uninhibited pmv were: $R^2 = 0.48$; slope = 7.8 μm s^{-1} nm^{-1} (95% confidence = 4.4 to 11.17 μm s^{-1} nm^{-1}); intercept = -155 μm s^{-1} (95% confidence = -760 to 449 μm s^{-1}), and AgSulf inhibited pmv $R^2 = 0.02$; slope = 0.2 μm s^{-1} nm^{-1} (95% confidence = -0.7 to 1.2 μm s^{-1} nm^{-1}); intercept = 90 μm s^{-1} (95% confidence = -90 to 271 μm s^{-1}).

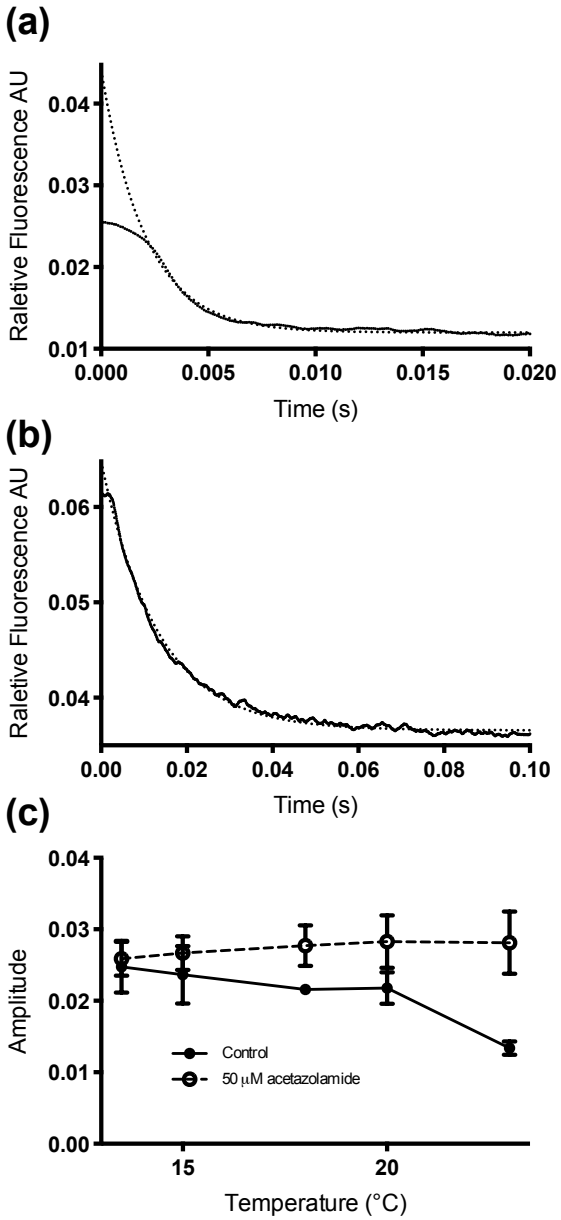

1042

1043 **Figure 5**. Time course of acidification in vesicles in response to CO_2 transport with and
1044 without acetazolamide at 13.5 ℃. (a) Time course of acidification in plasma membrane
1045 vesicles in response to CO_2 transport. The exponential fit is indicated by the dotted line. (b)
1046 With 50 μM acetazolamide (note change in time scale). (c) Comparison of the amplitude of
1047 the change in acidification in the presence or absence of acetazolamide at different
1048 temperatures. Mean +/- SEM (N=3).
1049

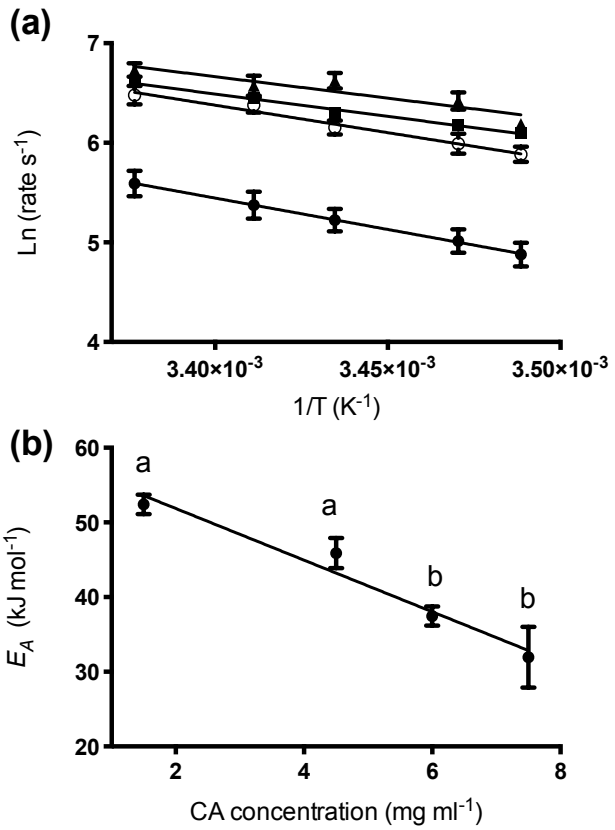

Figure 6. Temperature dependence of CO_2 acidification kinetics for pea leaf pmv and the effect of carbonic anhydrase (CA). (a) Arrhenius plots (13.5 ℃ to 23 ℃) of the rate of acidification at different intra-vesicular CA concentrations (solid circles 1.5 mg/ml; open circles 4.5 mg/ml; solid squares 6 mg/ml; solid triangles 7.5 mg/ml)). (b) Activation energy from the fits in (a) plotted against the intra-vesicular concentration of CA. Different letters indicate significant differences ($P < 0.05$). Mean +/- SEM (N=4).

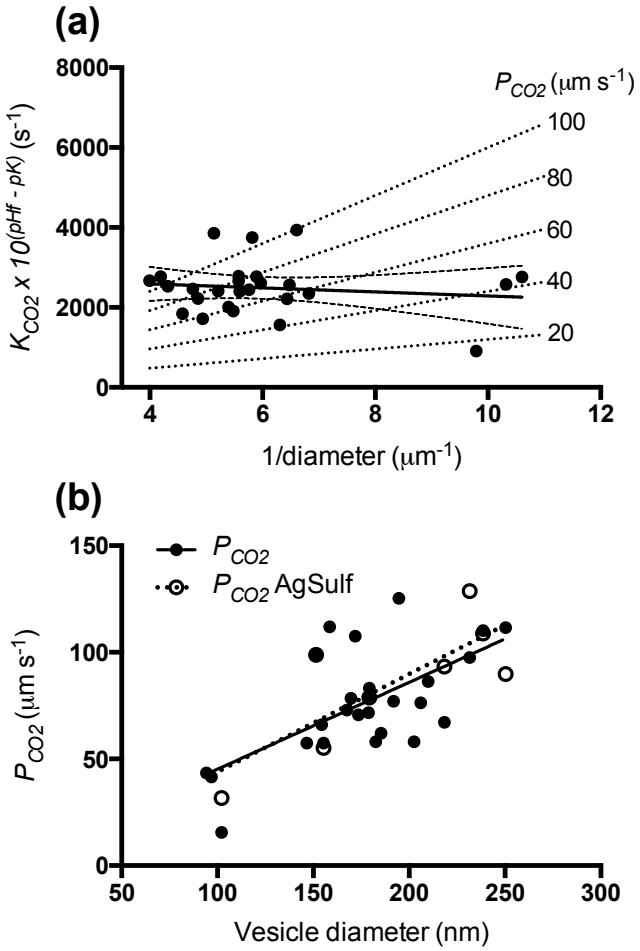

Figure 7. Effect of pea leaf vesicle diameter on K_{CO2} and P_{CO2}. (a) K_{CO2} x $10^{(pHf - pK)}$ is plotted against the inverse of vesicle diameter since according to Eq 2 if P_{CO2} is constant there should be a positive linear association between K_{CO2} x $10^{(pHf - pK)}$ and 1/diameter. These are shown for different values of P_{CO2} (dotted lines). A linear fit to the data is also shown (+/- 95% confidence interval) which is significantly different to that which would be obtained using the average P_{CO2}. (b) P_{CO2} as a function of vesicle diameter for all batches of pea leaf pmv (solid circles) and for those treated with AgSulf (open circles). The coefficients of the linear regression for the uninhibited pmvs were: R^2 = 0.40; slope = 0.41 μm s^{-1} nm^{-1} (95% confidence = 0.19 to 0.61 μm s^{-1} nm^{-1}); intercept = 4.5 μm s^{-1} (95% confidence = -33 to 42 μm s^{-1}), and AgSulf inhibited pmvs R^2 = 0.61; slope = 0.46 μm s^{-1} nm^{-1} (95% confidence = 0.09 to 0.82 μm s^{-1} nm^{-1}); intercept = -1.9 μm s^{-1} (95% confidence = -73 to 69 μm s^{-1}).

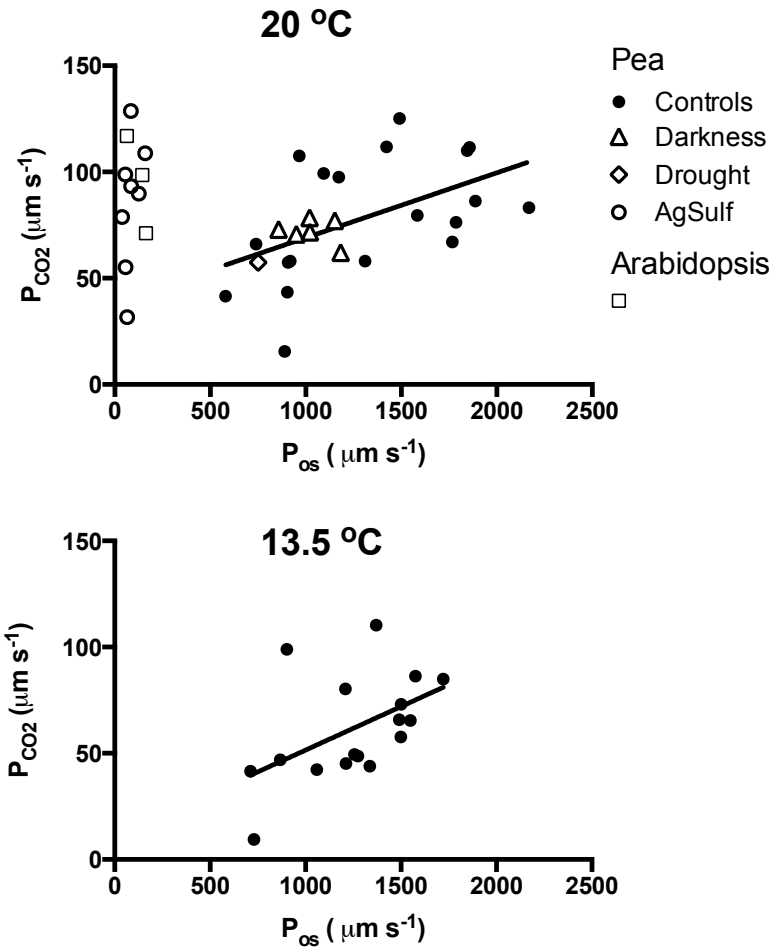

Figure 8. Relationship between P_{CO2} and P_{os} measured on the same batches of vesicles at 20 °C (a) and 13.5 °C (b). Some batches of plants were treated with darkness and drought as indicated by different symbols in (a). Also shown are the AgSulf treated pmv and *Arabidopsis* leaf pmv. The linear regression coefficients are: (a) Uninhibited 20 °C, R^2 = 0.27, slope = 0.03 (95% confidence = 0.009 to 0.05), intercept 38.6 μm s^{-1} (95% confidence = 10.9 to 66.2 μm s^{-1}); AgSulf inhibited 20 °C, R^2 = 0.18, slope = 0.32 (95% confidence = -0.35 to 0.99), intercept 58.8 μm s^{-1} (95% confidence = -3.3 to 120.8 μm s^{-1}) (b) 13.5 °C, R^2 = 0.25, slope = 0.04 (95% confidence = 0.002 to 0.08), intercept 10.5 μm s^{-1} (95% confidence = -39.9 to 60.9 μm s^{-1}).

Supplementary Material.

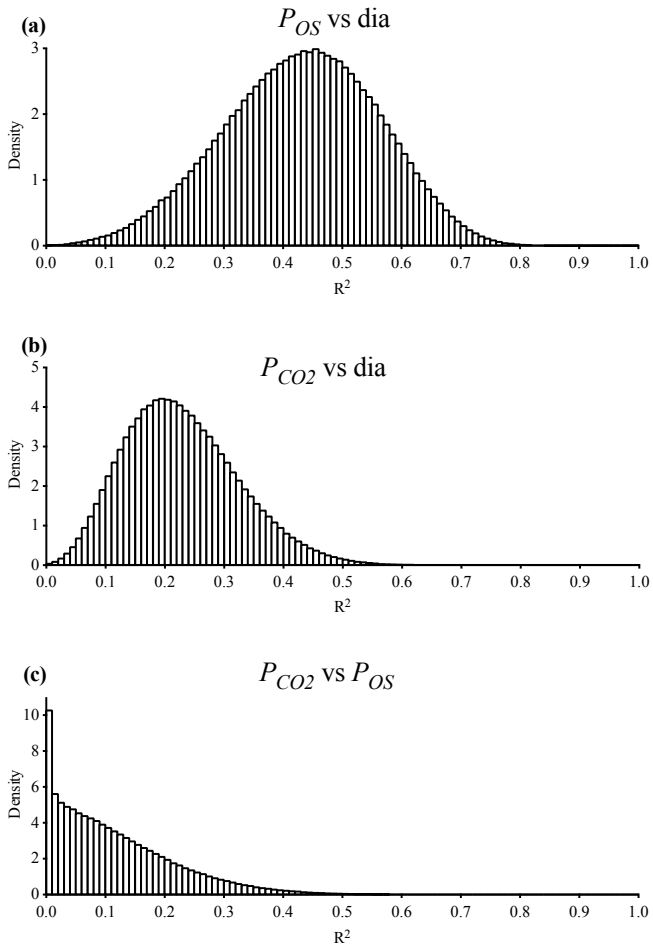

Figure S1 Probability densities for obtaining R^2 for correlation between P_{os} versus diameter (a), P_{CO2} versus diameter (b), and P_{CO2} versus P_{os} (c). Correlations may be expected between P_{os} or P_{CO2} and vesicle diameter since vesicle diameter is a parameter used in the calculation of the permeabilities. Similarly P_{CO2} and P_{os} may be correlated since they have the common factor of vesicle diameter. To assess this "common variable" effect simulations were carried out simulations using R (code available upon request) where rate constants used in the measurement of P_{os} and P_{CO2} were randomly varied about the mean with the same variance as measured. These randomly generated values where then used to calculate P_{os} and P_{CO2} using the measured vesicle diameters and the correlations examined for each random set (total 10^6). The Densities plotted are the percentage for obtaining a particular R^2 (in each bin). In the total population of P_{os} versus diameter there is a chance of 40.0057% to find a significant ($p <= 0.05$), positive slope with the observed R^2 of 0.4692 or above. In the total population of P_{CO2} versus diameter there is a chance of 4.6151% to find a significant ($p <= 0.05$), positive slope with the observed R^2 of 0.4043 or above. In the total population of P_{CO2} versus P_{os} there is a chance of 8.8061% to find a significant ($p <= 0.05$), positive slope with an R^2 of 0.27 or above. Moreover regarding the AgSulf inhibition data: In the total population of P_{os} versus diameter there is a chance of 0.0168% to find any positive slope with an R^2 of 0.02 or below.